

1 Volatiles in magmas related to the Campanian Ignimbrite eruption: experiments vs. natural findings.
2 Sara Fanara^{*1}, Roman E. Botcharnikov¹, Danilo M. Palladino², Franziska Adams¹, Julia
3 " Buddensieck¹, Andreas Mulch^{3,4}, Harald Behrens¹

5 ¹Institut für Mineralogie, Leibniz Universität Hannover, Callinstrasse 3, D-30167, Hannover,
6 Germany

7 ²Dipartimento di Scienze della Terra, Sapienza-Università di Roma, Piazzale Aldo Moro 5, 00185,
8 Roma, Italy

9 ³Biodiversität und Klima Forschungszentrum (BiK-F) & Senckenberg, Senckenberganlage 25
10 60325 Frankfurt/Main, Germany

11 ⁴Institut für Geowissenschaften, Goethe Universität Frankfurt, 60438 Frankfurt/Main, Germany

12

13 * Corresponding author.

14 Present address: Institut für Experimentelle und Angewandete Mineralogie, Georg-August
15 Universität Göttingen, Goldschmidt str.1, 37077, Göttingen

16 E-mail: Sara.Fanara@geo-uni-goettingen.de

17 Phone: 0049-0551-3933871

18 Fax: 0049-0551-393863

19

20

21

Abstract

22 The solubility of H₂O- and CO₂-bearing fluids in trachytic and trachybasaltic melts from erupted
23 magmas of the Campi Flegrei Volcanic District has been investigated experimentally at 1100°C and
24 1200°C, respectively, and at 100, 200, 300, 400 and 500 MPa. The solubility of H₂O in the
25 investigated melts varies between 3.48 ± 0.07 wt% at 100 MPa to 10.76 ± 0.12 wt% at 500 MPa in
26 trachytic melts and from 3.49 ± 0.07 wt% at 100 MPa to 9.10 ± 0.11 wt% at 500 MPa in
27 trachybasaltic melts. The content of dissolved CO₂ in melts coexisting with the most CO₂-rich fluid
28 phase increases from 281 ± 24 ppm at 100 MPa to 2710 ± 99 ppm at 500 MPa in trachyte, and from
29 727 ± 102 ppm at 100 MPa to 3565 ± 111 ppm at 500 MPa in trachybasalt.

30 Natural samples from the Campanian Ignimbrite eruption (trachyte) and from the Solchiaro eruption
31 (trachybasalt) were collected around the city of Naples and on Procida Island. Deuterium/Hydrogen
32 (D/H) ratios were analyzed in natural pumices pre-heated at different temperatures to remove water
33 adsorbed and/or imprinted by glass alteration processes. It has been determined that heating of the
34 glass to 350°C efficiently removes most of secondary water and the remaining concentrations
35 represent primary magmatic water preserved in the erupted material. Hydrogen isotope composition
36 (with δD values ranging between -70 ‰ and -110 ‰) and its correlation with bulk water content in
37 selected pumice samples of the Campanian Ignimbrite eruption are consistent with isotopic
38 fractionation between magmatic fluid and melt during degassing of erupting magma. Hence, the
39 H₂O and CO₂ contents in natural glasses from pumice samples are considered as minimum
40 estimates on volatile concentrations in the melt just prior to the eruption or at the fragmentation
41 event. The water contents in natural glasses vary from 0.83 ± 0.07 wt% to 3.74 ± 0.06 wt% for
42 trachytes from the Campanian Ignimbrite eruption and from 1.96 ± 0.06 wt% to 3.47 ± 0.07 wt%
43 for trachybasalts from the Solchiaro eruption. The CO₂ contents vary from 78 ± 120 ppm CO₂ to
44 1743 ± 274 ppm for trachytes from the Campanian Ignimbrite eruption and from 240 ± 293 ppm to
45 1213 ± 250 ppm for trachybasalts from the Solchiaro eruption.

2

46 A combination of natural and experimental data provides minimum pressure estimates for the
47 storage and ascent conditions of magmas. The Campanian Ignimbrite magma could have been
48 stored or ponded during its rising path at two different levels: a deeper one corresponding to depth
49 of about 8 to 15 km and a shallower one at about 1 to 8 km. Trachybasalts from Solchiaro erupted
50 from the deepest level of about 11 km with a storage or ponding level at around 2 to 8 km depth.
51 Although an uncertainty of at least a kilometer has to be considered in estimating storage or
52 ponding depths, these estimates point to significantly deeper magmatic sources for both eruptions as
53 those considered previously.

54

55 Keywords: Water, Carbon dioxide, Solubility, Hydrogen Isotopes, Trachyte, Trachybasalt, Campi
56 Flegrei Volcanic District, Campanian Ignimbrite eruption, Solchiaro eruption.

57

58

Introduction

59 The Campi Flegrei Volcanic District (CFVD) is located in southern Italy, immediately north-west
60 of the city of Naples. For more than 300 ka, this volcanic field was characterized by predominantly
61 explosive volcanic activity (Pappalardo et al., 2002). Nowadays this area still show evidence of
62 unrest: in the last 60 years the town of Pozzuoli (9 km NW of Naples) experienced spectacular
63 vertical ground movement on a scale of several meters, called bradyseism (Dvorak and
64 Mastrolorenzo, 1991; Yokoyama, 2006), accompanied by seismic swarms, fumarolic and
65 hydrothermal activities (e.g. Todesco 2009; Zollo et al. 2008; Pappalardo et al. 2008; Chiodini et
66 al., 2010, 2011; Aiuppa et al., 2013). Considering that more than 300,000 people live in the
67 polygenetic caldera of the Campi Flegrei, which includes part of the city of Naples itself (more than
68 1 million inhabitants), the predominantly explosive nature of eruptive activity and the present unrest

69 state of the volcano, the Campi Flegrei area is among those with the highest volcanic risk
70 worldwide.

71 The Campanian Ignimbrite (CI) was the most powerful eruption of the CFVD, yielding an
72 estimated volume up to 200 km³ (dense rock equivalent, DRE) with trachytic-phonolitic
73 composition (e.g. Civetta et al. 1997; Pappalardo et al. 2002; Self 2006; Arienzo et al. 2009; Di
74 Renzo et al., 2011; Scarpati et al., 2014). It was dated at approx. 39 ka, synchronous with significant
75 climate change (Fedele et al., 2002, 2003). The CI eruption has been largely investigated for
76 hundreds of years, being still an object of study today (Acocella, 2008; Fedele et al., 2008; Pabst et
77 al., 2008; Costa et al., 2012).

78 The vent location(s) and the stratigraphic sequence of the CI, as well as the shape and depth of its
79 magma chamber(s), are still under debate. Based on stratigraphic and geochemical investigations of
80 the deposits of the CI, Rosi and Sbrana (1987) and Fisher et al. (1993) suggested that the eruption
81 was accompanied by the formation of a caldera in the central area of Campi Flegrei. De Vivo et al.
82 (2001) and Rolandi et al. (2003) proposed a system of fractures north of Naples as source for the CI
83 eruption. Further studies of flow directions in pyroclastic deposits proximal to the CI vent(s)
84 determined by magnetic susceptibility measurements associated to the study of Bouguer anomalies
85 support the source location of the eruption within the Campi Flegrei area (Ort et al. 2003).

86 In addition to the reconstruction of the stratigraphic sequence of volcanic deposits from numerous
87 outcrops (e.g. Fedele et al., 2008), a core drilled in the northern part of the city of Naples showed
88 the superposition of a sequence of several pyroclastic flow units constituting the CI (Rosi et al.
89 1999; Pappalardo et al. 2002). The eruption started with a Plinian phase, responsible for SE-
90 dispersed pumice fallout. This phase was followed by the emplacement of ash and pumice flow
91 deposits and densely welded ignimbrites (Barberi et al. 1978). The lithic-rich Breccia Museo Unit is
92 interpreted as a co-ignimbrite lag breccia that marks the site and timing of caldera collapse during
93 the phase of maximum magma discharge rate (Rosi and Sbrana 1987; Fulignati et al. 2004).

94 Two different reconstructions of the magmatic feeding system of the Campanian Ignimbrite
95 eruption were presented in the last decades, proposing a batholithic or a sill-like magma reservoir.
96 In the first case, based on stratigraphic analysis combined with geochemical analysis of major and
97 trace elements of the pyroclastic deposits, it was suggested that the CI eruption was fed by a zoned
98 magma chamber with an upper volatile-rich phonolitic magma layer and a lower trachytic layer. A
99 recent 3-stage magmatic open system model based on isotopic investigation of the whole rock
100 samples, glasses and minerals (Arienzo et al. 2009, 2011) is in agreement with previous multi-stage
101 magma chamber models (Civetta et al. 1997; Signorelli et al. 2001; Pappalardo et al. 2002; De
102 Campos et al. 2004). It has been proposed that in the first stage juvenile magma was emplaced in
103 the middle crust and differentiated through crystal fractionation and assimilation of crustal material.
104 In the next stage this differentiated magma moved to a shallower crustal level and was stored in a
105 shallower magma chamber. In the final stage fresh trachytic magma was injected into the evolved
106 magma reservoir and formed the zoned magma chamber feeding the eruption. These models are
107 consistent with studies of melt inclusions in clinopyroxenes by Signorelli et al. (1999), Webster et
108 al. (2003), Fulignati et al. (2004) and Marianelli et al. (2006), which indicate that a relatively
109 homogeneous overheated trachytic magma resided within a relatively deep magma chamber and
110 evolved via fractional crystallization. Based on the information obtained from the analysis of matrix
111 juvenile glasses and melt inclusions, a range of temperatures from 850°C to 1080°C and pressures
112 from 40-60 MPa to 150 MPa was estimated. The latter indicate a magmatic storage region located
113 at 2 to 6 km depth. The variations in pressure were interpreted being caused by the movement of the
114 magma in the system.

115 Alternatively, Pappalardo et al. (2008) proposed another model based on partition coefficient
116 calculations, equilibrium mineral assemblages, juvenile glass compositions and texture to
117 reconstruct compositional, thermal and pressure gradients in the pre-eruptive reservoir, as well as
118 timing and mechanisms of evolution towards magma chamber overpressure and eruption. It has

119 been suggested that a high-temperature trachytic magma sill (1199°C) at a pressure of 250 MPa
120 cooled down rapidly at contact with cool country rocks to 1100°C. The suggested pressure of 250
121 MPa corresponds to a depth of about 9-10 km. The degree of melt undercooling abruptly increased
122 due to the thermal exchange between the trachytic magma body and the relatively cool country
123 rocks, driving a catastrophic and fast (10^2 years) in situ fractional crystallization and crustal
124 assimilation that produced a water oversaturated phonolitic cap and an overpressure in the chamber
125 that triggered the super-eruption. This model is supported by recent seismic studies that revealed an
126 anomalous low S-wave velocity zone at a depth of about 10 km. The seismic anomaly is interpreted
127 as a giant (500 km^3), sill-like magma reservoir between the metamorphic basement and the
128 overlying sedimentary rocks (Auger et al. 2001; De Natale et al. 2006; Zollo et al. 2008).

129 As shown, a generally accepted reconstruction of the depth and shape of the magmatic feeding
130 system just prior to the CI eruption is still missing and might be of crucial importance for volcanic
131 risk evaluation.

132 A main objective of this study is the determination of H_2O and CO_2 solubility in melts representing
133 synthetic analogues of the CFVD volcanics. Two compositional end-members of the CFVD were
134 investigated: the trachyte from the CI eruption and the trachybasalt from the Solchiaro volcanic
135 center (Procida) (14 Ka) (De Astis et al., 2004; Esposito et al., 2011, Mormone et al., 2011). The
136 experimental data are used for the interpretation of H_2O - CO_2 contents in glass inclusions, glass-
137 matrix and bulk rocks from natural samples, allowing a quantitative evaluation of the magmatic
138 pressure, and therefore depth, at which the natural samples were stored in the magma reservoir or
139 were undergoing the degassing processes during the magma ascent.

140 In the last decades, concentrations of H_2O and CO_2 species in aluminosilicates melts have been
141 experimentally investigated in a wide range of compositions, temperatures and pressures (Dixon et
142 al., 1995a; Tamic et al., 2001; Di Matteo et al., 2004; Behrens et al., 2004, 2009; Botcharnikov et
143 al., 2005a,b; 2006; Shiskina et al., 2010; Lesne et al., 2011a,b). It has been shown that H_2O and CO_2

144 solubility in MOR-basaltic, rhyolitic, as well as shoshonitic, compositions do not differ significantly
145 (Dixon et al., 1995 b,c; Berndt et al., 2002; Botcharnikov et al., 2005 a-b; Shishkina et al., 2010;
146 Vetere et al., 2011). However, high values of CO₂ solubility in calc-alkaline basalts and
147 phonotephritic melts were recorded (respectively, Moore, 2008; Behrens et al., 2009). This study
148 will contribute to extend the experimental data to alkali-rich trachytic and trachybasaltic
149 compositions for the pressure range between 100 and 500 MPa at 1100°C and 1200°C.

150 The obtained experimental datasets of H₂O-CO₂ solubility in CI trachytic and Solchiaro
151 trachybasaltic synthetic glasses were used to attempt the reconstruction of the depths and the shape
152 of the CI and Solchiaro magma storage systems prior to the eruption. In addition to the H₂O-CO₂
153 contents analyzed in melt inclusions from previous studies, the amount of H₂O and CO₂ in the
154 glass-matrix and in the bulk rock of well-characterized juvenile materials were analyzed in this
155 study. The juvenile natural samples of the CI eruption were collected around the caldera rim. The
156 juvenile samples of the Solchiaro deposit were collected at Procida, following the reconstruction of
157 the eruption by De Astis et al. (2004) and Esposito et al. (2011) to facilitate the comparison with
158 those studies. Analyses on glass matrix and bulk rock of juvenile samples (i.e., scoria, pumice and
159 ash) were largely used in previous studies, besides studies on melt inclusions, to estimate the
160 volatile contents of the eruptive products (Signorelli et al., 2001; Marianelli et al., 2006). In
161 particular, a comparison of post-eruptive volatile contents in matrix glasses with pre-eruptive
162 contents inferred from melt inclusions was used to assess the degassing rate during magma ascent
163 (Boissard et al., 2010 and references therein).

164 Recently, Giachetti and Gonnermann (2013) suggested that the matrix-glass water contents (up to
165 approx. 4 wt%) in samples from volcanic eruptions can originate from progressive rehydration of an
166 initially anhydrous glass sample during the time interval between deposition and sample collection.
167 To test for the presence of primary (magmatic) water and/or secondary (meteoric) water in the CI
168 samples, hydrogen isotope analyses were conducted on selected pumice samples. We suggest that

169 H₂O-CO₂ contents in matrix and bulk rock materials might be useful to define the minimum
170 pressure of the magma just prior to the eruption, in particular in the case of large eruptions such as
171 the CI, where well preserved melt inclusions are too few to be statistically representative of the
172 whole amount of magma involved.

173 **Sampling**

174 The locations of the natural samples used in this study are reported in Fig.1. The sampling was
175 aimed to record and successively compare the natural data from the whole CI succession exposed in
176 proximal settings, i.e. around the inferred CI caldera rim (Rosi and Sbrana, 1987) in CFVD and
177 Procida Island (SW sector of CFVD). The Basal Pumice Fallout was collected in the Taurano
178 Valley, about 30 km E of the city of Naples and 40 km E from the inferred CI vent area. Samples
179 from the upper part of the CI succession were collected around Naples at Ponti Rossi, Soccavo,
180 Acquamorta, Zaccaria and Spinelli.

181 A complete record of samples from the CI succession was collected at Procida, from the outcrops of
182 Punta della Lingua, Scotto di Carlo and Pozzo Vecchio. At Punta della Lingua, the CI eruptive
183 succession overlies an erosional discontinuity cut in the deposits of a local phreatomagmatic center
184 (>55 ka; Rosi et al., 1988) and includes, from bottom up: a stratified ash horizon, interpreted as the
185 equivalent of the “Plinian Pumice Fall Unit” (PPFU) in an upwind sector; a strongly welded spatter
186 deposit, referable to the “Piperno Unit” (PU), passing upward, through a lithic-rich spatter-bearing
187 deposit, to a coarse-grained, lithic-rich, pumice- and spatter-bearing breccia, an analogues of the
188 “Breccia Museo Unit” (BMU). The upper part of the CI succession is best exposed at Scotto di
189 Carlo, where the lithic-rich breccia becomes richer in pumice and grades upward to a massive
190 pumice flow deposit with ash matrix, related to the Upper Pumice Flow Unit” (UPFU) (Fig.2). The
191 ash fraction becomes largely dominant toward the top of the CI sequence. The stratified pyroclastic
192 surge deposits of the Solchiaro tuff ring crop out extensively at Procida on top of the CI.

193 Several samples of the Solchiaro eruption (TB-17; TB-18; TB-19) were collected at different
194 locations (Fig.1) and different stratigraphic heights, and are representative of the Solchiaro Unit II
195 according to the reconstruction of De Astis et al. (2004).

196 The main objects of the sampling were clasts of obsidian, spatter, white and grey pumice and the
197 pyroclastic flow matrix, as representative of the variety of juvenile products. The juvenile fractions
198 of the deposits were selected on the basis of cooling rate represented by sample textures to provide
199 suitable samples for bulk rock and glassy groundmass analyses. Therefore, the sample selection was
200 restricted to pumice from fallout deposits, proximal lithic-rich breccias, and well-quenched, distal
201 ignimbrite deposits. These samples were used in the petrological investigations of the CI and the
202 Solchiaro rocks.

203 **Experimental and analytical methods**

204 **Synthetic starting materials and experimental strategy**

205 The starting materials for the solubility experiments are a synthetic trachyte with composition close
206 to the CI pumice fall at Triflisco locality (OF17c1 sp; Civetta et al., 1997) and a synthetic
207 trachybasalt with composition close to Solchiaro III (Pro 6/2, pm; De Astis et al., 2004). These two
208 compositions represent end-members of the whole CFVD and are therefore fundamental to
209 understand the evolution of the magma for this volcanic district. The synthesis of the dry glasses
210 free of crystals and bubbles is described in Appendix I. The compositions of the glasses were
211 verified by a Cameca SX100 electron microprobe (Tab.1).

212 Dry glass powder was loaded in Au₈₀Pd₂₀ capsules (13 mm length, 3 mm diameter, 0.2 mm wall
213 thickness) with an appropriate amount of doubly distilled water and silver oxalate (Ag₂C₂O₄).
214 Ag₂C₂O₄ decomposes during heating and generates carbon dioxide. The amounts of H₂O and
215 Ag₂C₂O₄ loaded in each capsule were sufficient to ensure fluid-saturation at the investigated
216 conditions. Several sets of capsules were prepared with a starting mole fraction of water in the H₂O-

217 CO₂ system ($X_{\text{H}_2\text{O}}$) of 1, 0.8, 0.6, 0.4, and 0.2. The weight of each capsule was measured before and
218 after experiment to test for possible leakage. Solubility experiments were run in an Internally
219 Heated Pressure Vessel (IHPV) pressurized with Ar at 100, 200, 300, 400 and 500 MPa (± 5 MPa).
220 Temperatures were 1100°C and 1200°C ($\pm 10^\circ\text{C}$) for trachyte and trachybasalt, respectively. The
221 experimental duration was typically 24 h. Hydrogen fugacity was not adjusted in these experiments
222 and the redox conditions corresponded to that buffered by the intrinsic conditions of the IHPV
223 (Berndt et al., 2002). The oxygen fugacity in water-saturated capsules is typically 2.6 log units
224 above the Ni/NiO buffer under these conditions as determined by Schuessler et al. (2008) for the
225 IHPV used in this study. The samples were quenched isobarically with a cooling rate of about
226 150°C/s (Benne and Behrens, 2003). Glasses free of bubbles or quench crystals were obtained.

227 We performed an additional set of experiments for each composition to produce standards
228 necessary to calibrate the FTIR spectroscopy for the quantification of H₂O and CO₂ contents in the
229 glasses (see details below). In this case, about 150 mg of powdered glass and an appropriate amount
230 of H₂O and CO₂ were loaded into the capsules. To improve the homogeneity of the final product,
231 glass powder, H₂O and CO₂ were filled in the capsules in several steps. The annealing proceeded
232 according to the description above.

233 **Determination of fluids and glass composition in the experimental samples**

234 The compositions of H₂O-CO₂-bearing fluids were determined by weight-loss method after the
235 experiment. Each capsule was weighted, frozen in a liquid nitrogen bath and pierced with a needle.
236 After the piercing, the capsule was left at ambient temperature for few minutes to sublimate the
237 frozen CO₂ and weighted again to measure the released CO₂. The capsule was then stored in a
238 drying oven at 110°C for about five minutes and the weight of the capsule was periodically checked
239 until it remained constant. The samples with a water content above 6 H₂O wt% were carefully
240 treated with a specifically designed stepwise annealing. This procedure allowed measuring the
241 released H₂O. The determined mole fractions of H₂O ($X_{\text{H}_2\text{O}}^{\text{fl}}$) and CO₂ ($X_{\text{CO}_2}^{\text{fl}}$) in the fluid for
10

242 trachytic and trachybasaltic systems are reported in Tab.2 a-b, respectively. In the case of small
243 amounts of fluids, the main source of errors for the determinations of H₂O and CO₂ mole fractions
244 may be the incomplete separation of CO₂ and H₂O. The typical error of the balance used in this
245 study for the gravimetric measurements is about 0.10 mg.

246 The major element compositions of the experimental glasses were verified by electron microprobe
247 (measurement details are reported in Appendix I). No significant alkali loss was observed in
248 agreement with systematic tests performed by Stelling et al. (2008) for an alkali-rich basaltic glass.

249 The bulk water content of the experimental samples was measured by Karl-Fischer Titration (KFT)
250 after thermal dehydration (for details see Behrens et al., 1996). The data are reported in Tab.2 a b.
251 In the case of trachytic composition, the raw data were corrected by adding 0.10 wt% to account for
252 unextracted water in glasses after heating (Leschik et al., 2004). No correction was made for the
253 trachybasalt since dehydration is more efficient (Behrens et al., 2009) Using a CS analyzer ELTRA
254 800, the total carbon and sulfur contents were measured by combustion and subsequent IR
255 spectroscopy (CSA, for details see Appendix I). Doubly polished thin sections of post-experimental
256 samples were also prepared to analyze the H₂O and CO₂ contents using Fourier Transform Infrared
257 spectroscopy (FTIR) (for details see Appendix I).

258 **Characterization of the natural samples**

259 The collected juvenile samples (obsidian, scoria and pumice) were further selected based on their
260 macroscopic characteristics, i.e. samples with low to negligible degree of alteration were chosen.
261 The porosity of selected pumice clasts was determined to test its correlation with the water content
262 of the sample. A careful description of pumice selection and pre-analyses treatments, as well as
263 porosity measurements, is given in Appendix I.

264 Each piece of pumice was cut by a low-speed diamond saw in two halves for further analyses. The
265 bubble size distribution exposed on the cut area helps in tracing the number of the nucleation

266 event(s) that occurred before and during the cooling. A pumice showing bigger vesicles in the
267 center and smaller ones toward its rim surface was not considered for further investigations because
268 such bubble pattern indicates that the vesiculation process continued after magma fragmentation
269 during the pumice cooling. Only the pumices showing a homogeneous distribution of small vesicles
270 (possibly < 1 mm) were further considered.

271 One half of each sample was used to prepare a thin section. The major element composition of the
272 matrix glass was analyzed by electron microprobe following the conditions and the procedure
273 illustrated in Appendix I. The water content in the matrix glass was calculated “by difference”
274 according to Devine et al., 1995. The 2D-porosity for scoria and pumice samples was estimated by
275 analyzing back-scattered electron images by the software “ImageJ” (Appendix I - Tab. A1 a-b-c).

276 The remaining half of each natural sample was used for water and CO₂ determination with KFT and
277 CSA (Appendix I - Tab. A1 a-b-c). The water content analyzed on bulk rock pieces could be
278 affected by contributions from water trapped in the vesicles and by the presence of primary or
279 secondary hydrous minerals. Most of the samples were almost free of crystals (0-5%); in the case of
280 samples containing big phenocrysts (up to 1cm), these were manually removed before KFT
281 measurements. To test for contributions of volatiles trapped in closed vesicles, a portion of each
282 sample was crushed and sieved in several grain size (0-200 μm; 200-500 μm and >500 μm) and
283 finally analyzed by KFT and CSA.

284 To check for water bond in secondary minerals, such as zeolites, the remaining portions of some
285 samples were cut in several pieces that were stored in an oven overnight at different temperatures
286 (150°C, 200°C, 250°C, 300°C, 350°C and 400°C). The H₂O and CO₂ contents in the heat-treated
287 samples were analyzed with KFT and CSA (Appendix I - Tab. A1 a-b-c). To test if the water
288 present in the pumice glass is of either magmatic or meteoric origin, three pumice samples from the
289 Taurano Valley (i.e., from the initial stage of the CI eruption; PPFU) and four pumice samples from
290 Scotto di Carlo (UPFU; i.e., from the late stage of the CI eruption) were analyzed for hydrogen

291 isotopes. Hydrogen isotope measurements were performed at the Joint Goethe University – BiK-F
292 stable isotope facility Frankfurt (for further details see Appendix I).

293 **Results**

294 **Experimental products and glass composition**

295 The experimental conditions and the analytical results are reported in Tab.2 a-b. The experiments
296 were carried out at temperatures and pressures above the liquidus of the studied compositions and
297 samples were rapidly quenched. No crystals or bubbles were observed in the quenched glasses. The
298 microprobe analyses of the major element composition of the experimental samples (for details see
299 Appendix I – Tab.A2) show little differences from the composition of the starting material.

300 **Infrared spectroscopy and calibration of the absorption coefficients**

301 Typical NIR and MIR spectra for the determination of H₂O and CO₂ in experimental glasses are
302 reported in Appendix I - Fig. A1 a-b. For each sample, at least three spectra were collected in
303 different parts of the sample to test the homogeneity of the volatile distribution in the glasses. A
304 careful description of the obtained NIR and MIR spectra for trachytic and trachybasaltic glasses, as
305 well as the procedure to calculate the absorption coefficients, are reported in Appendix I. From the
306 available dataset, absorption coefficients of $\epsilon_{4500} = 1.19 \pm 0.02 \text{ L}\cdot\text{mol}^{-1}\cdot\text{cm}^{-1}$ and $\epsilon_{5200} = 0.98 \pm 0.03$
307 $\text{L}\cdot\text{mol}^{-1}\cdot\text{cm}^{-1}$ were derived for the bands at 4500 and 5200 cm^{-1} , respectively for trachyte. For
308 trachybasalt, the determined absorption coefficients are $\epsilon_{4500} = 0.83 \pm 0.02 \text{ L}\cdot\text{mol}^{-1}\cdot\text{cm}^{-1}$ and $\epsilon_{5200} =$
309 $0.79 \pm 0.04 \text{ L}\cdot\text{mol}^{-1}\cdot\text{cm}^{-1}$ (Fig. 3). We note that, for trachybasalt, almost identical low values for the
310 4500 cm^{-1} and the 5200 cm^{-1} bands were obtained, in agreement with the observations of previous
311 studies for other basaltic melt compositions (Ohlhorst et al., 2001; Mandeville et al., 2002; Behrens
312 et al., 2009; Shishkina et al., 2010). In the case of the trachytic composition, the obtained data agree
313 within errors with those determined by Fanara et al. (2013) for another trachyte from Campi
314 Flegrei, although the iron content in the latter trachyte was significantly higher.

315 Absorption coefficients for the carbonate peak of $\epsilon_{1430} = 413 \pm 13 \text{ L}\cdot\text{mol}^{-1}\cdot\text{cm}^{-1}$ and $\epsilon_{1430} = 292 \pm 11$
316 $\text{L}\cdot\text{mol}^{-1}\cdot\text{cm}^{-1}$ were derived for trachytic (Fig. 4-a) and trachybasaltic (Fig.4-b) glasses, respectively.
317 The latter agrees within errors with the determination for tholeiitic basalt glass (Shishkina et al.,
318 2010).

319 IR spectroscopic data show a homogeneous distribution of H₂O and CO₂ in the glasses, indicating
320 that the run duration was long enough to achieve equilibrium between the fluid phase and the melt.
321 At low concentrations, water is mostly present as OH⁻ groups in the quenched glass, whereas at high
322 water contents molecular H₂O dominates. Similar occurrence has been reported for various hydrous
323 silicate glasses (e.g., Bartholomew et al. 1980; Stolper 1982). Water was detected in all samples,
324 even in those for which water was not loaded in the capsule. As pointed out in previous papers (e.g.
325 Botcharnikov et al., 2006; Behrens et al., 2009), this is related to the reduction of ferric iron in the
326 melt induced by hydrogen permeation from the gas pressure medium into the capsule ($\text{Fe}_2\text{O}_3 + \text{H}_2 =$
327 $2\text{FeO} + \text{H}_2\text{O}$).

328 **Volatile contents in experimental and natural glasses**

329 The dependence of contents of H₂O and CO₂ in experimental glasses on fluid phase composition are
330 analyzed in details in Appendix I and shown in Fig. A2 (a-b-c-d) and in Tab.2 a-b. Water contents
331 of glasses determined by KFT and IR are in general in good agreement. Since water-rich samples
332 are sensitive to heating during sample preparation for IR, we have consistently used the KFT data in
333 the following discussions of solubility experiments. The amount of dissolved water in the
334 experimental melt in equilibrium with pure H₂O fluid increases from $3.48 \pm 0.07 \text{ wt}\%$ at 100 MPa
335 to $10.76 \pm 0.12 \text{ wt}\%$ at 500 MPa for trachyte (Fig. A2-a), and from $3.49 \pm 0.07 \text{ wt}\%$ at 100 MPa to
336 $9.10 \pm 0.11 \text{ wt}\%$ at 500 MPa for trachybasalt (Fig. A2-c). The content of CO₂ dissolved in the melts
337 equilibrated with the most CO₂ rich fluid phase ($0.79 < X_{\text{CO}_2}^{\text{fl}} < 0.94$ for trachyte; $0.72 < X_{\text{CO}_2}^{\text{fl}} <$
338 0.81 for trachybasalt) increases from $281 \pm 24 \text{ ppm}$ at 100 MPa to $2710 \pm 99 \text{ ppm}$ at 500 MPa in

339 trachyte (Fig. A2-b) and from 727 ± 102 ppm at 100 MPa to 3565 ± 111 ppm at 500 MPa in
340 trachybasalt (Fig. A2-d).

341 Table A1 a-b-c in Appendix I reports porosity and the H₂O and CO₂ contents in trachytic and
342 trachybasaltic natural samples from CI (a, on-land; b, Procida) and Solchiaro eruptions (c). Water
343 contents in matrix glasses of natural samples, derived by difference to the analytical total from
344 microprobe analyses, and 2D-porosities are described in details in Appendix I as well.

345 Pre-heating treatment of natural samples in the temperature range between 110°C and 400°C (see §
346 3.3) and application of specific heating program during KFT was used to distinguish primary,
347 magmatic water in the glass from primary or secondary water present in the closed vesicles and in
348 the altered glass. The water present in the closed vesicles, i.e. trapped along the vesicle walls in
349 hydrated layers, was estimated approx. 0.5 wt% as discussed in details in Appendix I. In Fig. 5 (i.e.
350 sample CI-LC P3) typical water release curves recorded by KFT are shown. Samples pre-heated
351 below 300°C show two peaks: one around 400°C and another one around 600°C. For the samples
352 heated overnight at 110°C (blue line, Fig.5), the fraction of water released at low temperatures was
353 estimated by integrating the titration curve up to the minimum between both peaks, and subsequent
354 scaling to the whole area below the titration curve; in this way, a water content of 1.21 wt% was
355 calculated, approx the 22% of the total water content (5.42 wt%). For the sample pre-heated at
356 350°C (red line, Fig.5) the peak at 400°C and its respective area (left of the dashed red line in Fig.5)
357 are strongly reduced: a water content of 0.23 wt% was calculated, approx. 7% of the total water
358 content (3.23 wt%). The sample pre-heated overnight at 400°C shows, beside a further decrease in
359 the peak at 400°C, a strong lowering of the main peak at 600°C. In Fig.6 the obtained bulk water
360 content from KFT analyses are represented as a function of the pre-heating temperature. It is shown
361 that a first drop in water concentration occurs between 200°C and 250°C and a second release of
362 water starts above 350°C. It is suggested that the first dehydration of the samples could be related to
363 the decomposition of the zeolitized glass. Zeolite minerals were not detected in our samples.

364 However, it is well known that the CI tuffs are rich in zeolites, in particular phillipsite and
365 chabazite, and sometimes present a zeolitization of the glass, without the nucleation of proper
366 zeolite crystals. Zeolites dehydrate at temperature between 190°C and 230°C (Hoss and Roy, 1960)
367 and part of the water released from the samples at $T < 300^\circ\text{C}$ could be attributed to the
368 decomposition of zeolites (Fig.6). The second dehydration of the samples above 350°C may be
369 related to a release of water bounded to the glass structure from the glass-matrix. Therefore, the
370 water content obtained after the heat treatment at 350°C was considered as representative of
371 primary magmatic water preserved in the natural samples. For the CI deposits sampled on-land
372 around the city of Naples, the amount of water after the second heat treatment reaches the
373 maximum in the PPFU (CI-LA-P2, 3.74 ± 0.06 wt% H_2O) and the minimum in the BMU (AM10B,
374 0.20 ± 0.06 wt% H_2O). Hence, it might be expected that the first deposits of the CI eruption may be
375 richer in volatiles than the last ones, consistent with the tapping of magma from different portions
376 of the reservoir through different source vents during a caldera-forming eruption (Masotta et al.,
377 2010; Palladino et al., 2014).

378 The CO_2 contents in the natural samples measured by CS-analyzer, show constant values before and
379 after the treatment at 350°C and reach a maximum of 1743 (± 274) ppm in the BPFU (CI-LA-P2)
380 and a minimum of 313 (± 301) ppm in the BMU (AM12 bis). For the CI products collected on the
381 island of Procida, the content of total H_2O varies between 1.43 ± 0.07 wt% (CF-CI 10-8b; CF-CI
382 10-10, UPFU) and 0.23 ± 0.06 wt% (CF-CI 10-3b, PU) in the sample annealed at 350°C. The CO_2
383 contents show values up to 2480 ± 101 ppm in the CF-CI 10-1b sample of the PU.

384 For the Solchiaro products sampled at Procida, the total H_2O varies between 3.47 ± 0.07 wt% (TB-
385 17-p2) and 0.60 ± 0.06 wt% (TB-19-p3) in the samples stored overnight at 350°C. The CO_2
386 contents show values up to 1293 ± 277 ppm (TB-17-p3).

387 Results of hydrogen isotope analyses of pumice samples collected in the Valle del Taurano and
388 Scotto di Carlo outcrops are listed in Tab.4 and illustrated in Fig.7. The average δD values range
16

389 from -62 ‰ (pre-heating at $T = 60^{\circ}\text{C}$ for 4h) to -76 ‰ (pre-heating at $T = 110^{\circ}\text{C}$ for 3h) and to -109
390 ‰ (pre-heating at $T = 350^{\circ}\text{C}$ for 3h) for the Valle del Taurano pumices and from -82 ‰ (pre-
391 heating at $T = 60^{\circ}\text{C}$ for 4h) to -85 ‰ (pre-heating at $T = 110^{\circ}\text{C}$ for 3h) and to -91 ‰ (pre-heating at
392 $T = 350^{\circ}\text{C}$ for 3h) for the Scotto di Carlo pumices. Bulk H_2O contents of the samples were
393 determined from the data of mass spectrometry for hydrogen isotopes by calibrating peak intensities
394 to reference materials with known water content (see also Appendix I). The obtained water contents
395 agree well with those determined by KFT (Tab.3).

396

Discussion

397

Solubility curves in trachytic and trachybasaltic melts

398 The volatile saturation diagrams of H_2O and CO_2 in trachytic and trachybasaltic glasses at
399 temperature of 1100°C and 1200°C , respectively, and pressure between 100 and 500 MPa are
400 shown in Fig.8 a-b. The isobars (solid lines in Fig.8) were plotted by an empirical fit of the
401 experimental data and represent the equilibrium concentrations of CO_2 and H_2O in the melt at given
402 pressure for the entire range of fluid composition. The isopleths of constant fluid composition (in
403 mole fractions of water; dashed lines in Fig.8) were calculated by interpolating and extrapolating
404 the composition of fluids measured in the experiments. Extrapolation of solubility trends to pure
405 CO_2 fluids has high uncertainty since oxygen fugacity decreases with decreasing water content of
406 the fluid and, hence, CO_2 fugacity decreases as well. Our datasets on the solubility of H_2O - CO_2
407 bearing fluids in trachytic and trachybasaltic melts show that up to 300 MPa the water solubility is
408 similar in both melts (Tab.2 a-b). At $P > 300$ MPa, H_2O solubility is higher in trachytic melts
409 compared to trachybasaltic melts. On the contrary, the CO_2 solubility is higher in the trachybasaltic
410 melts (727 ppm at 100 MPa) than in the trachytic melts (281 ppm at 100 MPa) at pressures below
411 300 MPa. At 500 MPa, the solubility of CO_2 in the trachybasaltic melt is approx. 24% higher than
412 in the trachyte melt. The solubility of H_2O - CO_2 bearing fluids from this study are in agreement with
413 the datasets of Shishkina et al. (2010, 2014) obtained for alkali-rich and alkali-poor mafic melts

17

414 and with the datasets of Vetere et al. (2011, 2014) obtained for alkali-rich shoshonitic and
415 phonotephritic melts. The H₂O concentrations of melts in equilibrium with pure H₂O fluids do not
416 differ significantly for these compositions and the isobaric solubility trends show similar curvatures.
417 The maximum amount of CO₂ soluble in the melts increase from trachyte (approx. 0.18 wt% at 400
418 MPa) to tholeiitic basalt (approx. 0.24 wt% at 400 MPa), trachybasalt (approx. 0.28 wt% at 400
419 MPa) and shoshonite (approx. 0.30 wt% at 400MPa). The main compositional differences between
420 the trachytic and trachybasaltic melts are the higher amounts of Ca and Mg in the trachybasalt and
421 the higher concentrations of Si and K in the trachyte.

422 Statistical analyses of experimental data from previous studies suggest that the chemical
423 composition and therefore the structure of melts play a fundamental role in CO₂ solubility (Iacono-
424 Marziano et al., 2012). In particular, it is clearly demonstrated that the CO₂ solubility increases with
425 the degree of melt depolymerization and with the amount of alkalis (e.g., Brooker et al., 1999,
426 2001a,b; Shishkina et al., 2014; Vetere et al., 2014). The NBO/T value for trachybasalt (0.71) is
427 higher than that for trachyte (0.17), explaining the higher CO₂ solubility determined for the
428 trachybasaltic melt. The nature of the cations bonded to the NBO is also critical: alkalis (Na+K)
429 bonded to NBO result in a strong enhancement of the CO₂ solubility, whereas Ca has a moderate
430 effect and Mg and Fe have the weakest effect (Iacono-Marziano et al., 2012, and references
431 therein). A recent study of Vetere et al. (2014) investigated the effect of alkalis on H₂O and CO₂
432 solubilities in alkali-rich silicate melts, confirming that, for constant NBO/T, Na promotes
433 carbonate incorporation stronger than K. On the other hand, Moore (2008) reported that Ca
434 concentration can strongly increase the CO₂ solubility in basaltic liquid. The CaO content in
435 trachybasalt (12.1 wt%) is three times higher than that in the trachyte (4.1 wt%), consistent with the
436 variation in CO₂ solubility between both compositions.

437 The experimental data on H₂O and CO₂ solubility in trachytic melts are compared with previous
438 numerical prediction models in Appendix I - Fig.A6.

439 **Implications for the Phlegrean Fields Volcanic District**

440 The volatile solubility diagrams shown in Fig.8 a-b were used for the interpretation of volatile
441 concentration data obtained from the natural trachytic and trachybasaltic melts from the CFVD,
442 relevant for the determination of magma storage conditions.

443 **What do we learn from analysis of melt inclusions and whole-rock juvenile samples?**

444 Although melt inclusions (MIs) in olivine can rapidly and selectively exchange water with the
445 matrix melt at magma storage conditions (e.g., Danyushevsky et al., 2002; Gaetani et al., 2012;
446 Portnyagin et al., 2008; 2012a,b), it can be assumed that MIs volatile exchange is limited during
447 rapid ascent of erupting magma. In this case, MIs should record the concentrations of H₂O and CO₂
448 in the magma reservoir at least just prior to eruption and/or at an uncertain time during magma
449 storage.

450 To gain information on the H₂O-CO₂ concentration in the melt at magma fragmentation (i.e. at the
451 eruption onset), we analyzed H₂O-CO₂ contents in pumice glasses. It is important to attest whether
452 the H₂O and the CO₂ contents detected in the pumice can be a reliable witness of the volatile
453 content in the pre-eruptive melt. Since H₂O is more abundant and mobile than CO₂, we will focus
454 on water, trying to establish its magmatic vs. meteoric origin, in the latter case resulting from
455 alteration processes. The juvenile samples, mostly pumice, analyzed in this study display high
456 values of porosity (at least >60%, but typically >70% - Appendix I – TabA1 a-b-c). We found a
457 broad positive correlation between porosity and matrix-glass water content, as shown in Fig.A5.
458 This correlation could be explained by syn-eruptive conditions, i.e. disequilibrium degassing where
459 the high decompression rate prevents the volatiles present in the glass-matrix to diffuse further into
460 the existing vesicles, or by post-eruptive rehydration processes. The key question is whether, or to
461 what extent, the data reflect prior- to syn-eruptive conditions. As shown in § 4.3, water can be
462 stored in the samples in different ways. Minor amounts of water can be trapped into the vesicles of

463 the closed porosity (i.e. up to 0.5 wt%). Significant amount of water can be stored in the altered,
464 zeolitized glass zones, being easily removed from the sample at low temperatures (<300°C; Fig.6)
465 due to zeolite decomposition, in particular in the presence of open pore system. The remaining
466 amount of water can be stored in the glass-matrix bounded to the glass structure (Fig.6). It is
467 suggested that the latter type corresponds to the pristine magmatic water present in the melt just
468 prior to the eruption. To support this hypothesis, D/H isotopic ratios were measured in the pumice
469 samples. Large isotopic fractionation between fluid and solid phases makes hydrogen isotopes a
470 very sensitive indicator of the water sources in nature.

471 The analyzed δD values of the pumice samples range from -62‰ to -114‰ and show correlation
472 with the bulk water content as illustrated in Fig.7. In order to unravel the contribution of meteoric
473 vs. magmatic water to these values, a comparison with isotopic signatures of meteoric and
474 magmatic water sources is presented. The δD value for meteoric waters in the Campi Flegrei area is
475 -33 ± 4 ‰ (Caprarelli et al., 1997; Panichi et al., 1999; Caliro et al., 2007 and references therein).
476 This value is converted into the expected isotopic composition of hypothetical glass hydrated by
477 meteoric waters using the fractionation factor of 0.967 determined for natural altered rhyolites by
478 Friedman et al. (1993). Such factor indicates that about 33‰ must be subtracted from the isotopic
479 value of meteoric water to obtain δD value of volcanic glass. In this conversion, we assumed that
480 the fractionation factor is not dependent on water content of the sample. The calculated range of
481 isotopic compositions in the samples hydrated by local meteoric waters is shown in Fig.7 as a blue
482 area.

483 The δD values for primary magmatic water range between -50 ‰ to -80 ‰ (see for instance,
484 Delmelle et al., 2000). Hydrogen isotope fractionation factors between fluid and melt are not very
485 well known for magmatic conditions. For instance, Richet et al. (1986) calculated a fractionation
486 between 8‰ and 25‰ for H₂O-albitic melt system at $870^\circ\text{C} < T < 1250^\circ\text{C}$ and 200 MPa. Pineau et
487 al. (1998) have proposed a relationship between hydrogen fractionation and water content of the

488 melt in the system H₂O fluid - basaltic andesite –at 1250°C and between 50 and 300 MPa. This
489 relationship is expressed as $\Delta D^{\text{fluid-melt}} = 18.1 \cdot (\text{H}_2\text{O, wt}\%)^{-0.5} + 15.7$ (where ΔD is a difference in
490 isotopic composition between fluid and melt and H₂O, wt% is the water content of the melt) and can
491 be used to estimate isotopic composition of melt, provided that the composition of coexisting fluid
492 is known. For the assumed range of δD values in magmatic waters of -50 to -80‰, the calculated
493 δD values of melts are lower by approximately 34 and 22‰ at 1 wt% and 8 wt%, respectively. The
494 correlation between δD and water content is not linear and the isotopic fractionation is more
495 pronounced at low water concentrations as illustrated by red field in Fig.7.

496 The isotopic data for pumice samples indicate that the isotopic signatures are inherited mostly from
497 magmatic source. Samples pre-heated to only 60°C show the highest contribution from meteoric
498 waters, presumably due to presence of adsorbed water or water impregnated in the samples by
499 alteration. Heating to 350°C effectively removes such meteoric water signature implying that water
500 contained in the glass structure, i.e., not released after heating treatment at 350°C, could be safely
501 considered as primary, magmatic water. One 350°C sample from Valle del Taurano is an obvious
502 outlier having also very large analytical uncertainty and it should be probably discarded.

503 The samples collected from the two sites, i.e., Valle del Taurano and Scotto di Carlo, show different
504 water contents and δD values (see Tab.3 and Fig.7). The Valle del Taurano samples show the
505 largest isotopic and concentration variations, even with dominating meteoric water signature in one
506 sample. On the contrary, the Scotto di Carlo samples do not evidence a considerable contribution
507 from meteoric waters. The observed differences between the two locations may have different
508 explanations: i) different eruption stages (i.e., early vs. late stage); ii) different emplacement
509 mechanisms (Plinian fall vs. pyroclastic current); iii) different magma/vent source(s); (iv) different
510 post-depositional conditions.

511 The most important conclusion derived from isotopic measurements is that pervasive alteration by
512 meteoric waters with a typical D/H isotopic ratio of the Neapolitan area can be removed by pre-
21

513 heating at 350°C. Thus, these samples can be used for the quantitative estimations of the volatile
514 budget in the magmas prior to eruption. However, we stress that these estimations can provide only
515 minimum values, due to magma degassing processes during the eruption and loss of volatiles from
516 the pumice.

517 **Pre-eruptive conditions of the Campanian Ignimbrite eruption**

518 The few existing studies on MIs in the CI products were mostly devoted to investigate processes
519 that occurred at various stages of the magmatic evolution of the CI and to characterize the magma-
520 withdrawal dynamics via major, minor and trace elements investigations (Signorelli et al., 1999;
521 Webster et al., 2003). Studies on phenocryst-hosted (mostly clinopyroxene) MIs in pumice clasts
522 erupted during different phases of the CI eruption show H₂O contents up to 6 wt% (Signorelli et al.,
523 2001; Marianelli et al., 2006), the water content in the MIs being in agreement with that in the glass
524 matrix. CO₂ content of MIs was below the detection limit of FTIR spectroscopy (20 ppm). From the
525 MIs data it has been inferred that a relatively homogeneous overheated trachytic magma resided
526 within a relatively deep magma chamber. Dissolved water contents in MIs indicate that prior to the
527 eruption the magma chamber underwent drastic changes related to differential upward movement of
528 magma. Decompression of the rising trachytic magma caused a decrease in water content by
529 degassing, resulting in magma crystallization, and emplacement of trachytic bodies at very shallow
530 depths (Marianelli et al., 2006). Moreover, the intrusion of a relatively mafic and volatile-rich
531 potassic shoshonite magma into the more evolved latite-trachyte magma body, with subsequent
532 mingling and mixing, could have played a significant role in triggering the eruption due to the input
533 of heat and volatiles (Webster et al., 2003).

534 The H₂O and CO₂ contents in natural pumice and ash glasses from the CI deposits, compared to the
535 new experimental dataset (Fig.9 a), were used to constrain the pressure of magma storage just prior
536 to the CI eruption. The CI samples from Procida show higher CO₂ and lower H₂O contents than
537 those collected from mainland Campi Flegrei around the city of Naples. An enrichment of CO₂ may

538 be explained with the assimilation of CaCO₃-rich wall rocks, consistent with magma tapping from
539 the peripheral portions of the reservoir through developing caldera ring faults.

540 The samples from Procida indicate the presence of at least two magma storage levels (Fig.9 a). In
541 fact, the early-erupted PPFU and PU (for abbreviations and stratigraphy see §2 and Fig.2) shows
542 volatile concentration values compatible with pressures above 400 MPa, i.e. deeper than 15 km.
543 Instead, the latest stages of the eruption (BMU and UPFU) show pressure values between 250 and
544 20 MPa, corresponding to a shallower magma storage between approx. 8 and 1 km of depth.
545 Samples from mainland Campi Flegrei show a systematic decrease in H₂O and CO₂ abundances in
546 the course of the CI eruption. In particular, the magma feeding the PPFU and PU was stored just
547 prior to the eruption at a pressure between approx. 410 and 220 MPa, which correspond, assuming a
548 pressure gradient of 27 MPa/km, to a depth of 15 – 8 km. The magma erupted later in the eruption,
549 during and after the caldera collapse (BMU and UPFU) was stored at pressures between 250 and
550 150 MPa, i.e. at depth between 9 and 5 km. It has to be emphasized that the pressures converted to
551 depths mentioned above are affected by an uncertainty of at least a kilometer.

552 **Pre-eruptive conditions of the Solchiaro eruption**

553 Esposito et al. (2011) and Mormone et al. (2011) focused recently on the major, minor and trace
554 elements and volatile contents of olivine-hosted MIs in the Solchiaro eruption products. Through
555 the correlation between H₂O-CO₂ contents of MIs (using the model of Papale et al. (2006) to
556 estimate the corresponding pressures) and the relative stratigraphic position of the investigated
557 samples, Esposito et al. (2011) suggested that a volatile-saturated magma initially ascended through
558 the crust from an original depth of at least 8 km. The magma ponded at 4 - 2 km depth prior to
559 eruption; the crystallization and the concomitant volatile exsolution from the saturated melt in the
560 shallow chamber would have triggered the Solchiaro eruption. As the eruption proceeded, the
561 Solchiaro magma continued to ascend through the crust to a final storage depth of about 1 km
562 (Esposito et al., 2011; see Fig. 9b, red dots).

563 In this study, the H₂O-CO₂ contents in MIs (Esposito et al., 2011; Mormone et al., 2011) and in
564 scoria and pumice glasses from juvenile samples (this study) are reported in comparison with
565 experimental data in Fig.9 b. The H₂O-CO₂ concentration detected in the matrix glasses from the
566 Solchiaro juvenile samples indicate a similar pressure range compared to the MIs from Esposito et
567 al. (2011) and Mormone et al. (2011). However, the water content in pumice glasses varies largely
568 between 2.37 wt% and 0.17 wt% (Tab.3 c), different from the H₂O content in the MIs from
569 Esposito et al. (2011) that show an approx. constant value ranging from 1.10 wt% to 1.40 wt%. In
570 an open degassing system, the concentration of water in the melt may follow the isopleth, which
571 could explain the trend of water in the MIs. By comparing the water contents in MIs (Fig.9 b) with
572 the isopleths derived from the experimental values (Fig.8 b), a misfit is evident, particularly for low
573 CO₂ contents. As mentioned above, the low concentration of H₂O in MIs could reflect storage of the
574 magma in a relatively low pressure region i.e. re-equilibration of MIs with the surrounding melt.
575 Our experimental dataset may help constraining the pressure at which the MIs reported in Esposito
576 et al. (2011) and Mormone et al. (2011) were stored in the Solchiaro feeder magma in the range of
577 approx. 50 – 300 MPa. In particular, concerning the H₂O-CO₂ concentration in juvenile matrix
578 glasses, just prior to the Solchiaro eruption, most of the magma was at pressure between 150 and 50
579 MPa, i.e. at depth of 5 – 2 km. A few scoria clasts show a deepest provenance, from a region at
580 approx. 9 km depth (260 MPa). Assuming a pressure gradient of 27 MPa/km, we estimate the
581 deepest magma source below 11 km depth, with the main magma storage between 8 and approx. 2
582 km depth. Also in this case, the estimated depths are affected by an uncertainty of at least a
583 kilometer.

584

Acknowledgments

585 This research has been supported by a research grant within the scope of the Integrated Continental
586 Drilling Program ICDP (SPP1006) – Campi Flegrei (CFDDP). Andreas Mulch acknowledges
587 support through the LOEWE funding program (Landes-Offensive zur Entwicklung

588 wissenschaftlich-ökonomischer Exzellenz) of Hesse's Ministry of Higher Education, Research, and
589 the Arts.

590 The authors acknowledge Otto Dietrich for the excellent work on the preparation of samples for
591 analyses. We would like to thank Dr. Anika Husen for her help with the IHPV apparatus and Wanja
592 Dziony and Eric Wolff for the advices on electron microprobe analyses. Half of the natural samples
593 were collected with the help of Gabriele Macchi-Ceccarani and Simone Righi under the supervision
594 of Prof. Raffaello Trigila. The pumices in the Taurano Valley were sampled under the discerning
595 guide of Prof. Giuseppe Rolandi. We thank J. Fiebig (Goethe Universität Frankfurt) for stable
596 isotope laboratory support. This paper benefited of many discussions with Dr. Giuseppe
597 Mastrolorenzo, Prof. Benedetto De Vivo and Dr. Claudia Cannatelli concerning the Campi Flegrei
598 volcanic system that greatly improved the quality of this manuscript. We thank Dr. Zoltan Zajacz
599 and an unknown reviewer for the careful correction, discussion and improvement of the original
600 manuscript.

601

Figure capture

602 **Fig.1** (a) Digital elevation model of the Campi Flegrei Volcanic District; (b) the outset map show
603 an enlarged view of the Campi Flegrei area. The sample locations of the CI eruption are indicated
604 by red stars; the sample locations of the Solchiaro eruption are indicated by blue stars.

605 **Fig.2** Schematic stratigraphic correlations of Campanian Ignimbrite deposit as it outcrops around
606 the city of Naples and on the Island of Procida. Locations are reported in Fig.1 b.

607 **Fig.3** Calibration plot for determination of molar absorption coefficients for the OH combination
608 band at 4500 cm^{-1} and H_2O combination band at 5200 cm^{-1} . Solid lines were obtained by the linear
609 regression of the corresponding data in plot. Intercepts of the lines with the axes define the molar
610 absorption coefficients for OH (x-axes) and H_2O (y-axes). For comparison, data for basalt from
611 Ohlhorst et al. (2001), tholeitic basalt from Shishkina et al. (2010), shoshonite from Vetere et al.

612 (2011), and trachyte from Fanara et al. (2013) are shown. The tangent baseline was used to extract
613 absorbance values.

614 **Fig.4** Calibration plot for the determination of the absorption coefficient for the carbonate band at
615 1430 cm^{-1} for trachyte (a) and for trachybasalt (b) Bulk CO_2 content was determined by CS
616 analyses.

617 **Fig.5** Water release curves determined by KFT of hydrous natural trachytic pumice heated
618 overnight at 100°C (blue line), 350°C (red line) and 400°C (black line). The grain size of the
619 powder was $> 500\mu\text{m}$. The curves are normalized to a sample weight of 20.00 mg. The heating rate,
620 which strongly influences the curves, is taken into account in the definition of the temperatures. The
621 dashed blue and red lines divide the portions of the trends interpreted as adsorbed water from those
622 interpreted as water bonded in the glass structure, respectively for the 110°C and 350°C curves.

623 **Fig.6:** Bulk water content in the sample LC P3 analyzed by KFT as a function of the temperature at
624 which the sample was heated overnight. The grain size of the analyzed sample is $> 500\mu\text{m}$. Dashed
625 lines indicate the range of temperatures up to which the most common zeolites are stable. The
626 decrease in water content with T increase up to 250°C indicates a loss of adsorbed or secondary
627 water (incorporated in zeolites) from the samples. A plateau in water content at T between 250 and
628 350°C is interpreted as water bonded to the glass structure and hence representing “primary”
629 magmatic water. This type of water can be extracted from the glass by further heating to $T>400^\circ\text{C}$.

630 **Fig.7** Relationship between isotopic composition of hydrogen (δD) and bulk water content for
631 Campanian Ignimbrite pumice samples from Valle del Taurano (VdT) and Scotto di Carlo (SdC).
632 Pumice samples were pre-heated at 60°C , 110°C , and 350°C for 4h before isotopic measurements
633 as noted in the legend. In most samples, the error bars represent precision of the methods because
634 the reproducibility errors were typically lower than the analytical uncertainty. Blue field illustrates
635 calculated isotopic composition of pumice samples equilibrated with local meteoric waters

636 assuming a fractionation factor of 0.967 after Friedman et al. (1993). The isotopic composition of
637 meteoric water ($-33\pm 4\%$; Caliro et al., 2007 and reference therein) is converted into isotopic
638 composition of altered glass by subtracting 33%. Red field corresponds to the expected isotopic
639 composition of magmatic melts in equilibrium with magmatic fluids as a function of water content
640 dissolved in the melt.

641 **Fig.8** Solubility plot for H₂O and CO₂ in (a) trachytic and (b) trachybasaltic melts. The solid lines
642 represent isobars plotted by an empirical fit of the experimental data. The dashed lines show
643 isopleths of constant fluids composition in equilibrium with the melt.

644 **Fig.9** Comparison of the experimental dataset (Tab.2 a-b) with (a) juvenile glass matrix from CI
645 (this study – Appendix I - Tab.A1 a-b) and (b) with juvenile glass matrix (this study - Appendix I -
646 Tab.A1 c) and MIs (Esposito et al., 2011, in red; Mormone et al., 2011, in blue) from Solchiaro
647 eruption.

648

References

649 Acocella, V. (2008) Activating and reactivating pairs of nested collapses during caldera-forming
650 eruptions: Campi Flegrei (Italy). *Geophysical Research Letters* 35, doi:10.1029/2008GL035078.

651 Aiuppa, A., Tamburello, G., Di Napoli, R., Cardellini, C., Chiodini, G., Giudice, G., Grassa, F., and
652 Pedone, M. (2013) First observations of the fumarolic gas output from a restless caldera:
653 Implications for the current period of unrest (2005-2013) at Campi Flegrei. *Geochemistry*
654 *Geophysics Geosystems*, DOI: 10.1002/ggge.20261.

655 Aranovitch, L.Y., and Newton, R.C., (1996). H₂O activity in concentrated NaCl solutions at high
656 pressures and temperatures measured by the brucite-periclase equilibrium. *Contrib. Mineral. Petrol.*,
657 125.

- 658 Arienzo, I., Civetta, L., Heumann, A., Wörner, G., and Orsi, G. (2009) Isotopic evidence for open
659 system processes within the Campanian Ignimbrite (Campi Flegrei – Italy) magma chamber.
660 *Bulletin of Volcanology*, 71, 285-300.
- 661 Arienzo, I., Heumann, A., Wörner, G., Civetta, L., and Orsi, G. (2011) Processes and timescales of
662 magma evolution prior to the Campanian Ignimbrite eruption (Campi Flegrei, Italy). *Earth and*
663 *Planetary Science Letters* 306, 217-228.
- 664 Auger, E., Gasparini, P., Virieux, J., and Zollo, A. (2001) Seismic evidence of an extended
665 magmatic sill under Mt. Vesuvius. *Science* 294, 1510-1512.
- 666 Balcone-Boissard, H., Boudon, G., and Villemant, B. (2011) Textural and geochemical constraints
667 on eruptive style of the 79 AD eruption at Vesuvius. *Bull. Volcanol.*, 73, pp. 279–294
- 668 Barberi, F., Innocenti, F., Lirer, L., Munno, R., Pescatore, T., and Santacroce, R. (1978) The
669 campanian ignimbrite: a major prehistoric eruption in the Neapolitan area (Italy). *Bulletin*
670 *Volcanologique* 41, 1, 10-31.
- 671 Bartholomew, R.F., Butler, B.L., Hoover, H.L., and Wu, C.K. (1980) Infrared spectra of a water-
672 containing glass. *J. Am. Ceram. Soc.* 63, 481–485.
- 673 Behrens, H., Romano, C., Nowak, M., Holtz, F., and Dingwell, D.B. (1996) Near-infrared
674 spectroscopic determination of water species in glasses of the system $MA\text{Si}_3\text{O}_8$ (M = Li, Na, K):
675 An interlaboratory study. *Chemical Geology*, 128, 1-4, 41-63.
- 676 Behrens, H., Ohlhorst, S., Holtz, F., and Champenois, M. (2004) CO_2 solubility in dacitic melts
677 equilibrated with $\text{H}_2\text{O}-\text{CO}_2$ fluids—Implications for modeling the solubility of CO_2 in silicic
678 melts. *Geochimica et Cosmochimica Acta*, 68, 4687–4703.

- 679 Behrens, H., Misiti, V., Freda, C., Vetere, F., Botcharnikov, R.E., and Scarlato, P. (2009) Solubility
680 of H₂O and CO₂ in ultrapotassic melts at 1200 and 1250 °C and pressure from 50 to 500 MPa.
681 American Mineralogist, 94, 105–120.
- 682 Benne, D., and Behrens, H. (2003) Water solubility in haplobasaltic melts. European Journal of
683 Mineralogy, 15, 803-814.
- 684 Berndt, J., Liebske, C., Holtz, F., Freise, M., Nowak, M., Ziegenbein, D., Hurkuck, W., and
685 Koepke, J. (2002) A combined rapid-quench and H₂-membrane setup for internally heated pressure
686 vessels: Description and application for water solubility in basaltic melts. American Mineralogist,
687 87, 1717-1726.
- 688 Blank, J.G., and Brooker, R.A. (1994) Experimental studies of carbon dioxide in silicate melts:
689 solubility, speciation and stable isotope behavior. In M.R. Carroll and J.R. Holloway, Eds.,
690 Volatiles in Magmas, 30, 157–186. Reviews in Mineralogy, Mineralogical Society of America
691 Chantilly Virginia.
- 692 Botcharnikov, R.E., Freise, M., Holtz, F., and Behrens, H. (2005a) Solubility of C-O-H mixtures in
693 natural melts: New experimental data and application range of recent models. Annals of
694 Geophysics, 48, 633–646.
- 695 Botcharnikov, R.E., Koepke, J., Holtz, F., McCammon, C., and Wilke, M. (2005b) The effect of
696 water activity on the oxidation and structural state of Fe in a ferro-basaltic melt. Geochimica et
697 Cosmochimica Acta, 69, 5071–5085.
- 698 Botcharnikov, R.E., Behrens, H., and Holtz, F. (2006) Solubility and speciation of C–O–H fluids in
699 andesitic melt at T=1100–1300 °C and P=200 and 500 MPa. Chemical Geology, 229, 125–143.

- 700 Brooker, R.A., Kohn, S.C., Holloway, J.R., McMillan, P.F., and Carroll, M.R. (1999) Solubility,
701 speciation and dissolution mechanisms for CO₂ in melts on the NaAlO₂–SiO₂ join. *Geochimica*
702 *Cosmochimica Acta*, 63, 3549–3565.
- 703 Brooker, R.A., Kohn, S.C., Holloway, J.R., and McMillan, P.F. (2001a) Structural controls on the
704 solubility of CO₂ in silicate melts. Part I: bulk solubility data. *Chemical Geology*, 174, 225-239.
- 705 Brooker, R.A., Kohn, S.C., Holloway, J.R., and McMillan, P.F. (2001b) Structural controls on the
706 solubility of CO₂ in silicate melts Part II: IR characteristics of carbonate groups in silicate glasses.
707 *Chemical Geology*, 174, 241-254.
- 708 Burnham, C. W., (1994) Development of the Burnham model for prediction of H₂O solubility in
709 magmas. *Mineralogical Society of America, Reviews in Mineralogy*, v. 30, 123–129.
- 710 Caliro S., G. Chiodini, R. Moretti, R. Avino, D. Granieri, M. Russo, and J. Fiebig (2007) The origin
711 of the fumaroles of La Solfatara (Campi Flegrei, South Italy). *Geochim. Cosmochim. Acta*, 71-12,
712 3040.
- 713 Caprarelli, G., Tsutsumi, M., and Turi, B., (1997) Chemical and isotopic signatures of the basement
714 rocks from the Campi Flegrei geothermal field (Naples, southern Italy): inferences about the origin
715 and evolution of its hydrothermal fluids. *Journal of Volcanology and Geothermal Research*, 76, 63-
716 82
- 717 Chiodini, G., Caliro, S., Cardellini, C., Granieri, D., Avino, R., Baldini, A., Donnini, M., and
718 Minopoli, C. (2010) Long-term variations of the Campi Flegrei, Italy, volcanic system as revealed
719 by the monitoring of hydrothermal activity. *Journal of Geophysical Research*, 115,
720 doi:10.1029/2008JB006258.

- 721 Chiodini, G., Avino, R., Caliro, S., and Minopoli, C. (2011) Temperature and pressure gas
722 geoindicators at the Solfatara fumaroles (Campi Flegrei). *Annals of Geophysics*, 54-2, doi:
723 10.4401/ag-5002.
- 724 Civetta, L., Orsi, G., Pappalardo, L., Fisher, R.V., Heiken, G., and Ort, M. (1997) Geochemical
725 zoning, mingling, eruptive dynamics and depositional processes – the Campanian Ignimbrite,
726 Campi Flegrei caldera, Italy. *Journal of Volcanology and Geothermal Research*, 75, 183-219.
- 727 Costa, A., Folch, A., Macedonio, G., Giaccio, B., Isaia, R., and Smith, V.C. (2012) Quantifying
728 volcanic ash dispersal and impact of the Campanian Ignimbrite super-eruption. *Geophysical
729 Research Letters* 39, doi:10.1029/2012GL051605.
- 730 Danyushevsky, L.V., McNeill, A.W., and Sobolev, A.V. (2002) Experimental and petrological
731 studies of melt inclusions in phenocrysts from mantle-derived magmas: An overview of techniques,
732 advantages and complications. *Chemical Geology*, 183, 5–24.
- 733 De Astis, G., Piochi, M. and Pappalardo, L. (2004). Procida volcanic history: new insights in the
734 evolution of the Phlegraean Volcanic District (Campania, Italy). *Bulletin of Volcanology*, 66, 622-
735 641.
- 736 De Campos, C.P., Dingwell, D.B., and Fehr, K.T. (2004) Decoupled convection cells from mixing
737 experiments with alkaline melts from Phlegrean Fields. *Chemical Geology*, 213, 227-251.
- 738 Delmelle P., Bernard A., Kusakabe M., Fischer T.P., and Takano B. (2000) Geochemistry of the
739 magmatic–hydrothermal system of Kawah Ijen volcano, East Java, Indonesia. *Journal of
740 Volcanology and Geothermal Research*, 97, 1–4, 31-53.
- 741 De Natale, G., Troise, C., Pingue, F., Mastrolorenzo, G., Pappalardo, L., Battaglia, L., and Boschi,
742 E. (2006) The Campi Flegrei caldera: unrest mechanisms and hazard. In: Troise, C., De Natale, G.,

- 743 Kilburn, C.R.J., (eds) Mechanisms of activity and unrest at large calderas. Geol. Soc. London Spec.
744 Publ., 269,159–171.
- 745 Devine, J. D., Gardner, J. E., Brack, H. P., Layne, G. D. and Rutherford, M. J. (1995) Comparison
746 of microanalytical methods for estimating H₂O contents of silicic volcanic glasses. American
747 Mineralogist, 80, 319-328.
- 748 De Vivo, B., Rolandi, G., Gans, P.B., Calvert, A., Bohrson, W.A., Spera, F.J., and Belkin, H.E.
749 (2001) New constraints on the pyroclastic eruptive history of the Campanian volcanic Plain (Italy).
750 Mineralogy and Petrology, 73, 47-65.
- 751 Di Matteo, V., Carroll, M.R., Behrens, H., Vetere, F., and Brooker, R.A. (2004) Water solubility in
752 trachytic melts. Chemical Geology, 213, 187–196.
- 753 Di Renzo, V., Arienzo, I., Civetta, L., D'Antonio, M., Tonarini, S., Di Vito, M.A., and Orsi, G.
754 (2011) The magmatic feeding system of the Campi Flegrei caldera: Architecture and temporal
755 evolution. Chemical Geology, 281, 227-241.
- 756 Dixon, J.A., and Pan, V. (1995a) Determination of the molar absorptivity of dissolved carbonate in
757 basanitic glass. American Mineralogy, 80, 1339-1342.
- 758 Dixon, J.E., Stolper, E.M., and Holloway, J.R. (1995b) An experimental study of water and carbon
759 dioxide solubilities in mid-ocean ridge basaltic liquids. Part I: Calibration and solubility models.
760 Journal of Petrology, 36, 1607–1631.
- 761 Dixon, J.E., and Stolper, E.M. (1995c) An experimental study of water and carbon dioxide
762 solubilities in Mid-Ocean Ridge Basaltic liquids. Part II: applications to degassing. Journal of
763 Petrology, 36, 1633–1646.
- 764 Dvorak, J.J., and Mastrolorenzo, G. (1991) The mechanisms of recent vertical crustal movements in
765 Campi Flegrei caldera, southern Italy. Geol. Soc. Am. Spec. Pap., 263, 47.

- 766 Esposito, R., Bodnar, R.J., Danyushevsky, L.V., De Vivo, B., Fedele, L., Hunter, J., Lima, A., and
767 Shimizu, N. (2011) Volatile evolution of magma associated with the Solchiaro eruption in the
768 Phlegrean Volcanic District (Italy). *Journal of Petrology*, 52, 12, 2431-2460.
- 769 Fanara, S., Behrens, H., and Zhang, Y. (2013) Water diffusion in potassium-rich phonolitic and
770 trachytic melts. *Chemical Geology*, 346, 149-161.
- 771 Fedele, F.G., Giaccio, B., Isaia, R., and Orsi, G., (2002). Ecosystem Impact of the Campanian
772 Ignimbrite Eruption in Late Pleistocene Europe. *Quaternary Research*, 57, 3, 420-424.
- 773 Fedele, F.G., Giaccio, B., Isaia, R., and Orsi, G., (2003) The Campanian Ignimbrite eruption,
774 Heinrich event 4 and the Palaeolithic change in Europe: a high-resolution investigation. In: A.
775 Robock, C. Oppenheimer (Eds.), "Volcanism and Earth's Atmosphere", 139AGU Geophysical
776 Monograph, Washington, USA (2003), 301–325
- 777 Fedele, L., Scarpati, C., Lanphere, M., Melluso, L., Morra, V., Perrotta, A., and Ricci, G. (2008)
778 The Breccia Museo formation, Campi Flegrei, southern Italy: geochronology, chemostratigraphy
779 and relationship with the Campanian Ignimbrite eruption. *Bulletin of Volcanology*, 70, 1189-1219.
- 780 Fisher, R.V., Orsi, G., Ort, M., and Heiken, G. (1993) Mobility of large-volume pyroclastic flow –
781 emplacement of the Campanian Ignimbrite, Italy. *Journal of Volcanology and Geothermal*
782 *Research*, 56, 205-220.
- 783 Friedman I., Gleason J., Sheppard R.A., and Gude A.J. (1993) Deuterium Fractionation as Water
784 Diffuses into Silicic Volcanic Ash. *Climate Change in Continental Isotopic Record*. Geophysical
785 Monograph, 78, 321-323.
- 786 Fulignati, P., Marianelli, P., Proto, M., and Sbrana, A. (2004) Evidences for disruption of a
787 crystallizing front in a magma chamber during caldera collapse: an example from the Breccia

- 788 Museo Unit (Campanian Ignimbrite eruption, Italy). *Journal of Volcanology and Geothermal*
789 *Research*, 133, 141-155.
- 790 Gaetani, G.A., O'Leary, J.A., Shimizu, N., Bucholz, C.E., and Newville, M. (2012) Rapid
791 reequilibration of H₂O and oxygen fugacity in olivine-hosted melt inclusions. *Geology*, 40, 915-
792 918.
- 793 Giachetti T., and Gonnermann H.M. (2013) Water in volcanic pyroclast: Rehydration or incomplete
794 degassing? *Earth and Planetary Science Letters*, 369–370, 317-332.
- 795 Giordano, D., Nichols, A.R.L., and Dingwell, D.B. (2005) Glass transition temperatures of natural
796 hydrous melts: a relationship with shear viscosity and implications for the welding process. *Journal*
797 *of Volcanology and Geothermal Research*, 142, 105-118.
- 798 Hoss, H., and Roy, R. (1960) Zeolite Studies III: on natural phillipsite, gismondite, harmotome,
799 chabazite and gmelinite. *Mineralogie and Petrographie* b, 389-408.
- 800 Iacono-Marziano G., Morizet Y., Le Trong E., and Gaillard F. (2012) New experimental data and
801 semi-empirical parameterization of H₂O–CO₂ solubility in mafic melts. *Geoch. Cosmoch. Acta*, 97,
802 15, 1-23.
- 803 Leschik, M., Heide, G., Frischat, G.H., Behrens, H., Wiedenbeck, M., Wagner, N., Heide, K.,
804 Geißler, H., and Reinholz, U. (2004) Determination of H₂O and D₂O contents in rhyolitic glasses.
805 *Physic and Chemistry of Glasses*, 45, 4, 238-251.
- 806 Lesne,P., Scaillet,B., Pichavant,M., Iacono-Marziano,G. and Beny, J.M. (2011a) The H₂O solubility
807 of alkali basaltic melts: an experimental study. *Contributions to Mineralogy and Petrology*, 162,
808 133-151.
- 809 Lesne, P., Scaillet, B., Pichavant,M. and Beny, J.M. (2011b) The carbon dioxide solubility in alkali
810 basalts: an experimental study. *Contributions to Mineralogy and Petrology*, 162, 153-168.

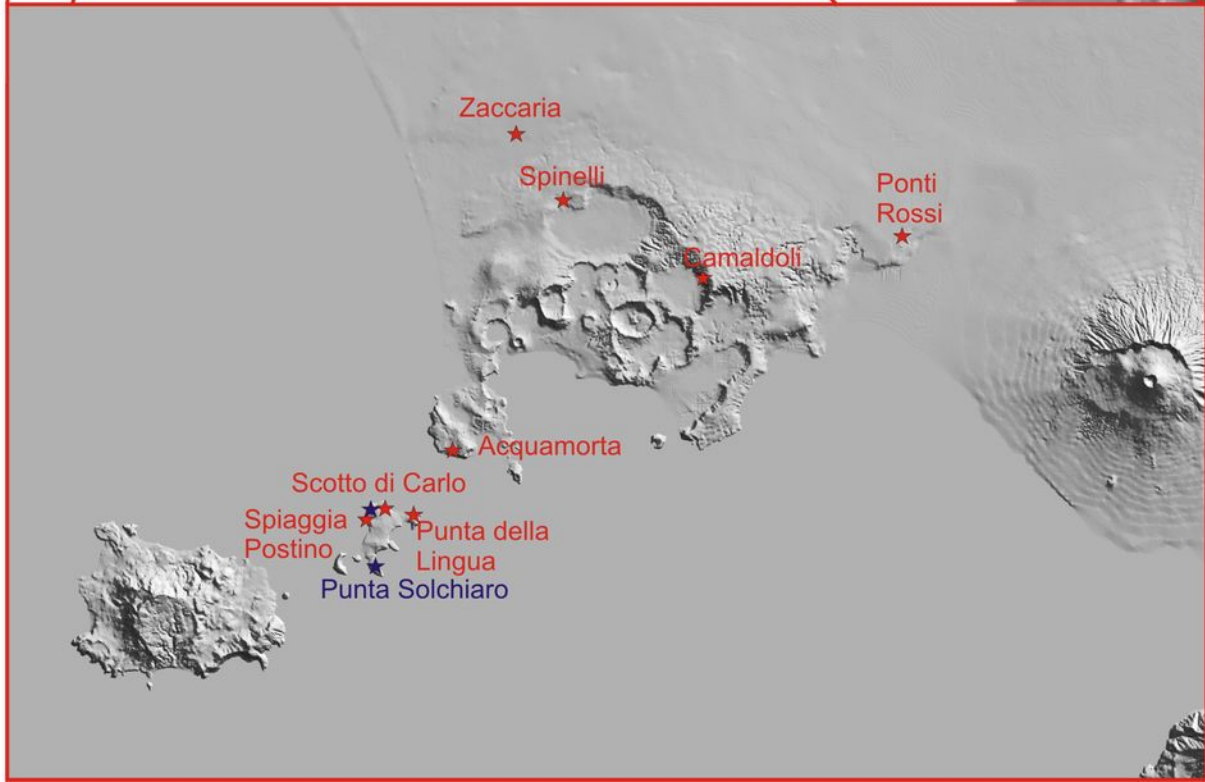
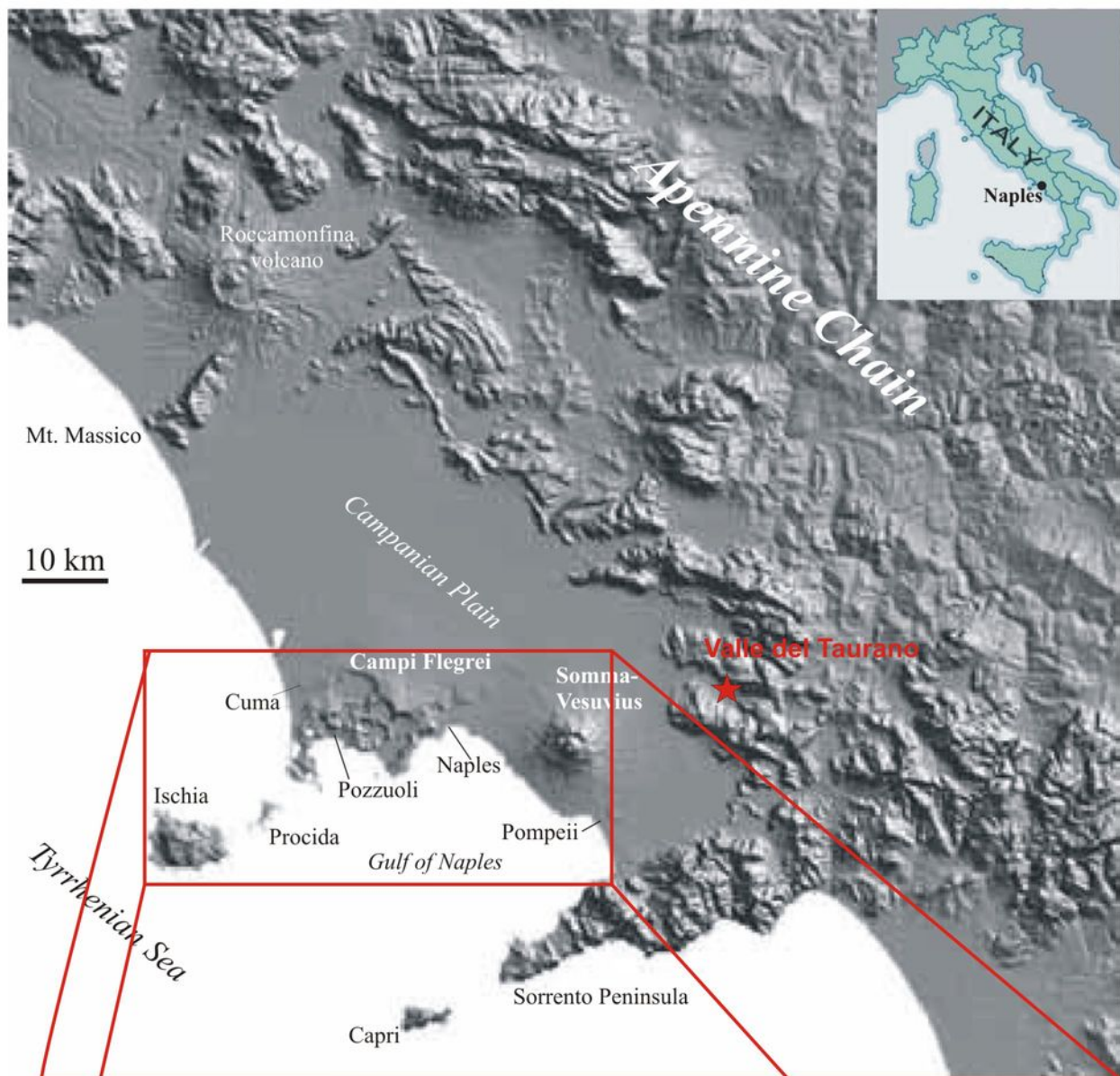
- 811 Mandeville, C.W., Webster, J.D., Rutherford, M.J., Taylor, B.E., Timbal, A., and Faure, K. (2002)
812 Determination of molar absorptivities for infrared absorption bands of H₂O in andesitic glasses.
813 American Mineralogist, 87, 813-821.
- 814 Marianelli, P., Sbrana, A., and Proto, M. (2006) Magma chamber of the Campi Flegrei
815 supervolcano at the time of eruption of the Campanian Ignimbrite. Geological Society of America,
816 34, 11, 937-940.
- 817 Masotta, M., Gaeta, M., Gozzi, F., Marra, F., Palladino, D.M., and Sottili, G. (2010) H₂O- and
818 temperature-zoning in magma chambers: the example of the Tufo Giallo della Via Tiberina
819 eruptions (Sabatini Volcanic District, central Italy). Lithos, 118, 1-2, 119-130.
- 820 Moore, G. (2008) Interpreting H₂O and CO₂ contents in melt inclusions; constraints from solubility
821 experiments and modeling. In: Putirka, K.D. and Tepley, F.J., III (eds) Minerals, Inclusions and
822 Volcanic Processes. Mineralogical Society of America and Geochemical Society, Reviews in
823 Mineralogy and Geochemistry, 69, 333-362.
- 824 Mormone, A., Piochi, M., Bellatreccia, F., De Astis, G., Moretti, R., Della Ventura, G., Cavallo, A.,
825 and Mangiacapra, A. (2011) A CO₂-rich magma source beneath the Phlegraean Volcanic District
826 (Southern Italy): evidence from a melt inclusion study. Chemical Geology, 287, 66-80.
- 827 Newman, S., and Lowenstern, J.B. (2002) VolatileCalc: a silicate melt-H₂O-CO₂ solution model
828 written in Visual Basic for excel. Computational Geosciences, 28, 597-604.
- 829 Ohlhorst, S., Behrens, H., and Holtz, F. (2001) Compositional dependence of molar absorptivities
830 of near-infrared OH-and H₂O bands in rhyolitic to basaltic glasses. Chemical Geology, 174, 5-20.
- 831 Ort, M., Orsi, G., Pappalardo, L., and Fisher, R.V. (2003) Emplacement processes in a far-traveled
832 dilute pyroclastic current: anisotropy of magnetic susceptibility studies of the Campanian
833 Ignimbrite. Bulletin of Volcanology, 65, 55-72.

- 834 Pabst, S., Wörner, G., Civetta, L., and Tesoro, R. (2008) Magma chambre evolution prior to the
835 Campanian Ignimbrite and Neapolitan Yellow Tuff eruptions (Campi Flegrei, Italy). *Bulletin of*
836 *Volcanology*, 70, 8, 961-976.
- 837 Palladino, D.M., Gaeta, M., Giaccio, B., and Sottili, G. (2014) On the anatomy of magma chamber
838 and caldera collapse: the example of trachy-phonolitic explosive eruptions of the Roman Province
839 (central Italy). *J. Volcanol. Geotherm. Res.*, 281, 12-26.
- 840 Panichi, C., and Volpi, G., (1999) Hydrogen, oxygen and carbon isotope ratios of Solfatara
841 fumaroles (Phlegrean Fields, Italy): further insight into source processes. *J. Volcanol. Geotherm.*
842 *Res.*, 91, 2-4, 321-328.
- 843 Papale, P., Moretti, R., and Barbato, D. (2006) The compositional dependence of the saturation
844 surface of H₂O+CO₂ fluids in silicate melts. *Chemical Geology*, 229, 78-95.
- 845 Pappalardo, L., Civetta, L., De Vita, S., Di Vito, M., Orsi, G., Carandente, A., and Fisher, R.V.
846 (2002) Timing of magma extraction during the Campanian Ignimbrite eruption (Campi Flegrei
847 Caldera). *Journal of Volcanology and Geothermal Research*, 114, 479-497.
- 848 Pappalardo, L., Ottolini, L., and Mastrolorenzo, G. (2008) The Campanian Ignimbrite (southern
849 Italy) geochemical zoning: insight on the generation of a super-eruption from catastrophic
850 differentiation and fast withdrawal. *Contribution to Mineralogy and Petrology*, 156, 1-26.
- 851 Pineau, F., Shilobreeva, S., Kadik, A., and Javoy, M. (1998) Water solubility and D/H fractionation
852 in the system basaltic andesite-H₂O at 1250°C and between 0.5 and 3 kbars. *Chemical Geology*,
853 147, 1-2, 173-184
- 854 Portnyagin, M., Almeev, R., Matveev, S., and Holtz, F. (2008) Experimental evidence for rapid
855 water exchange between melt inclusions in olivine and host magma. *Earth and Planetary Science*
856 *Letters*, 272, 3-4, 541-552.

- 857 Portnyagin, M.V., Hoernle, K., and Mironov, N.L. (2012a) Contrasting compositional trends of
858 rocks and olivine-hosted melt inclusions from Cerro Negro volcano (Central America): implications
859 for decompression-driven fractionation of hydrous magmas. *International Journal of Earth Sciences*,
860 DOI 10.1007/s00531-012-0810-3.
- 861 Portnyagin, M., Hoernle, K., Storm, S., Mironov, N., van den Bogaard, C., and Botcharnikov, R.
862 (2012b) H₂O-rich melt inclusions in fayalitic olivine from Hekla volcano: Implications for phase
863 relationships in silicic systems and driving forces of explosive volcanism on Iceland. *Earth and
864 Planetary Science Letters*, 357-358, 337-346.
- 865 Richet, P., Roux, J., and Pineau, F. (1986) Hydrogen isotope fractionation in the system H₂O-liquid
866 NaAlSi₃O₈: new data and comments on D/H fractionation in hydrothermal experiments. *Earth and
867 Planetary Science letters*, 78, 115-120.
- 868 Richet, P., Whittington, A., Holtz, F., Behrens, H., Ohlhorst, S., and Wilke, M. (2000) Water and
869 the density of silicate glasses. *Contribution to Mineralogy and Petrology*, 138, 337-347.
- 870 Rolandi, G., Bellucci, F., Heizler, M.T., Belkin, H.E. and De Vivo, B. (2003) Tectonic controls on
871 the genesis of ignimbrites from the Campanian Volcanic Zone, southern Italy. *Mineralogy and
872 Petrology*, 79, 3-31.
- 873 Rosi, M., and Sbrana, A. (1987) Phlegrean Fields. *CNR Quaderni della Ricerca Scientifica*, 114, 9,
874 175.
- 875 Rosi, M., Sbrana, A., and Vezzoli, L. (1988) Stratigrafia delle Isole di Procida e Vivara. *Bollettino
876 GNV*, IV, 500-525.
- 877 Rosi, M., Vezzoli, L., Castelmennano, A., and Grieco, G. (1999) Plinian pumice fall deposito f the
878 Campanian Ignimbrite eruption (Phlegrean Fields, Italy). *Journal of volcanology and Geothermal
879 Research*, 91, 179-198.



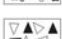

- 880 Scarpati, C., Sparice, D., and Perrotta, A. (2014) A crystal concentration method for calculating
881 ignimbrite volume from distal ash-fall deposits and a reappraisal of the magnitude of the
882 Campanian Ignimbrite. *J. Volcanol. Geotherm. Res.*, 280, 67-75.
- 883 Scholze, H. (1960) Zur Frage der Unterscheidung zwischen H₂O Molekeln und OH-Gruppen in
884 Gläsern und Mineralen. *Naturwissenschaften*, 47, 226–227.
- 885 Scholze, H. (1966) Gases and water in glass. *Glass Industry*, 47, 546–551, 622–628.
- 886 Schuessler, J.A., Botcharnikov, R.E., Behrens, H., Misiti, V., and Freda, C. (2008) Oxidation state
887 of iron in hydrous phono-tephritic melts. *American Mineralogist*, 93, 1493–1504.
- 888 Self, S. (2006) The effects and consequences of very large explosive volcanic eruptions.
889 *Philosophical Transactions of the Royal Society A*, 364, 2073-2097.
- 890 Shishkina, T., Botcharnikov, R.E., Holtz, F., Almeev, R., and Portnyagin, M.V. (2010) Solubility of
891 H₂O and CO₂-bearing fluids in tholeiitic basalts at pressures up to 500 MPa. *Chemical Geology*,
892 277, 115–125.
- 893 Shishkina, T.A., Botcharnikov, R.E., Holtz, F., Almeev, R.R., Jazwa, A.M., and Jakubiak, A.A.
894 (2014) Compositional and pressure effects on the solubility of H₂O and CO₂ in mafic melts.
895 *Chemical Geology*, 388(0), 112-129.
- 896 Signorelli, S., Vaggelli, G., Francalanci, L., and Rosi, M. (1999) Origin of magmas feeding the
897 Plinian phase of the Campanian Ignimbrite eruption, Phlegrean Fields (Italy): constraints based on
898 matrix-glass and glass-inclusion compositions. *Journal of Volcanology and Geothermal Research*,
899 91, 199-220.
- 900 Signorelli, S., Vaggelli, G., Romano, C., and Carroll, M.R. (2001) Volatile element zonation in
901 Campanian Ignimbrite magmas (Phlegrean Fields, Italy): evidence from the study of glass
902 inclusions and matrix glasses. *Contributions to Mineralogy and Petrology*, 140, 543-553.

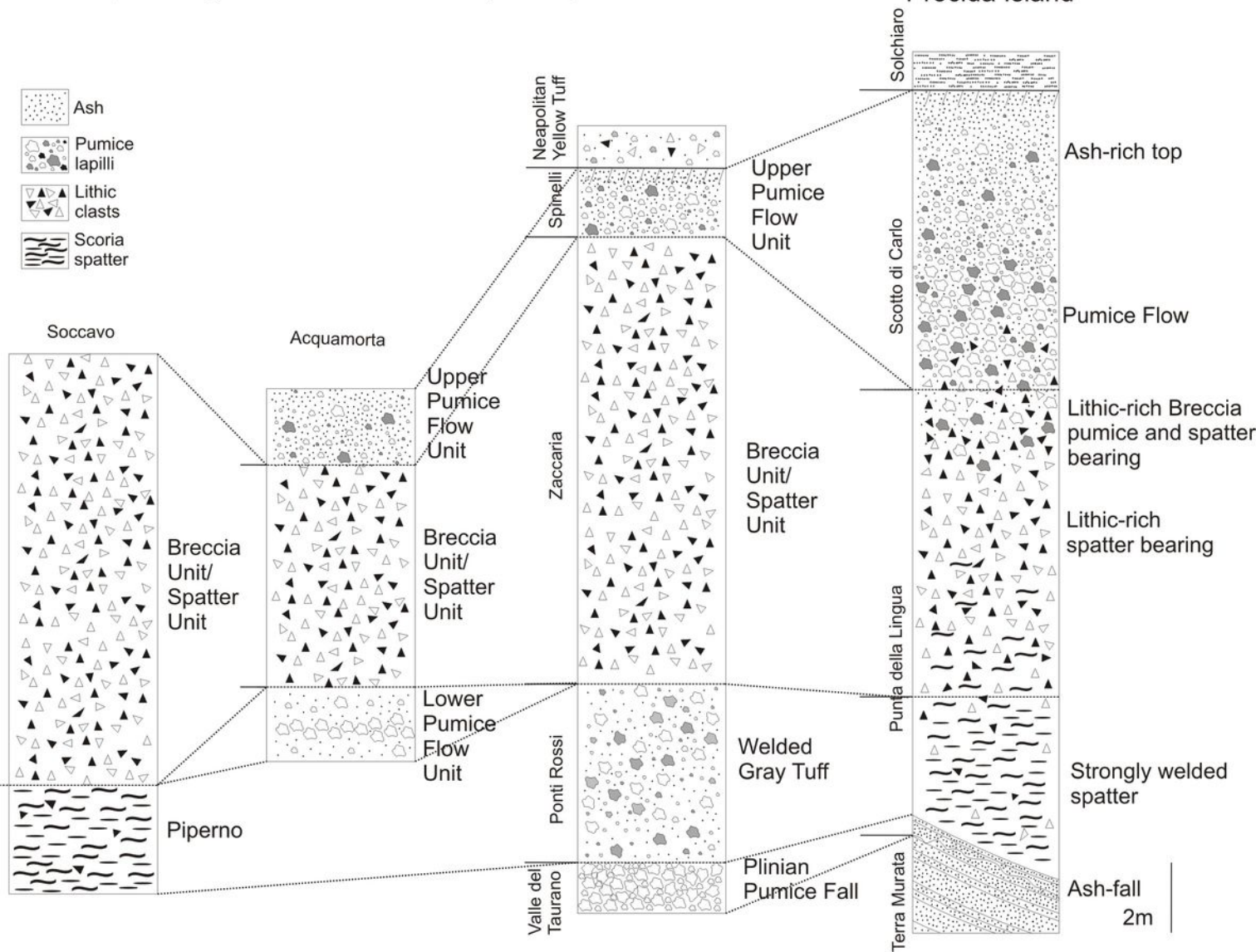
- 903 Stelling J., Botcharnikov R.E., Beermann O., and Nowak M. (2008) Solubility of H₂O- and
904 chlorine-bearing fluids in basaltic melt of Mount Etna at T=1050–1250 °C and P=200 MPa.
905 *Chemical Geology*, 256, 3–4, 102-110.
- 906 Stolper, E. (1982) Water in silicate glasses: an infrared spectroscopic study. *Contrib. Mineral.*
907 *Petrol.*, 81, 1–17.
- 908 Tamic, N., Behrens, H., and Holtz, F. (2001) The solubility of H₂O and CO₂ in rhyolitic melts in
909 equilibrium with a mixed CO₂-H₂O fluid phase. *Chemical Geology*, 174, 333–347.
- 910 Todesco, M. (2009) Signals from the Campi Flegrei hydrothermal system: Role of a magmatic
911 source of fluids. *Journal of Geophysical Research*, 114, doi:10.1029/2008JB006134.
- 912 Vetere, F., Botcharnikov, R.E., Behrens, H., Holtz, F., and De Rosa, R. (2011) Solubility of H₂O
913 and CO₂ in shoshonitic melts at 1250°C and pressure from 50 to 400 MPa. *Journal of Volcanology*
914 *and Geothermal Research*, 202, 251–261.
- 915 Vetere, F., Holtz, F., Behrens, H., Botcharnikov, R., and Fanara, S. (2014) The effect of alkalis and
916 polymerization on the solubility of H₂O and CO₂ in alkali-rich silicate melts. *Contributions to*
917 *Mineralogy and Petrology*, 167(5), 1-17.
- 918 Webster, J.D., Raia, F., Tappen, C., and De Vivo, B. (2003) Pre-eruptive geochemistry of the
919 ignimbrite-forming magmas of the Campanian Volcanic Zone, southern Italy, determined from
920 silicate melt inclusions. *Mineralogy and Petrology*, 79, 99-125.
- 921 Yokoyama, I. (2006) The 1969-1985 Pozzuoli event and active volcanisms. *Proc. Japan Acad.*,
922 *Ser.B*, 82, 121-126.
- 923 Zollo, A., Maercklin, N., Vassallo, M., Dello Iacono, D., Virieux, J., and Gasparini, P. (2008)
924 Seismic reflections reveal a massive melt layer feeding Campi Flegrei caldera. *Geophysical*
925 *Research Letters* 35, doi:10.1029/2008GL034242.

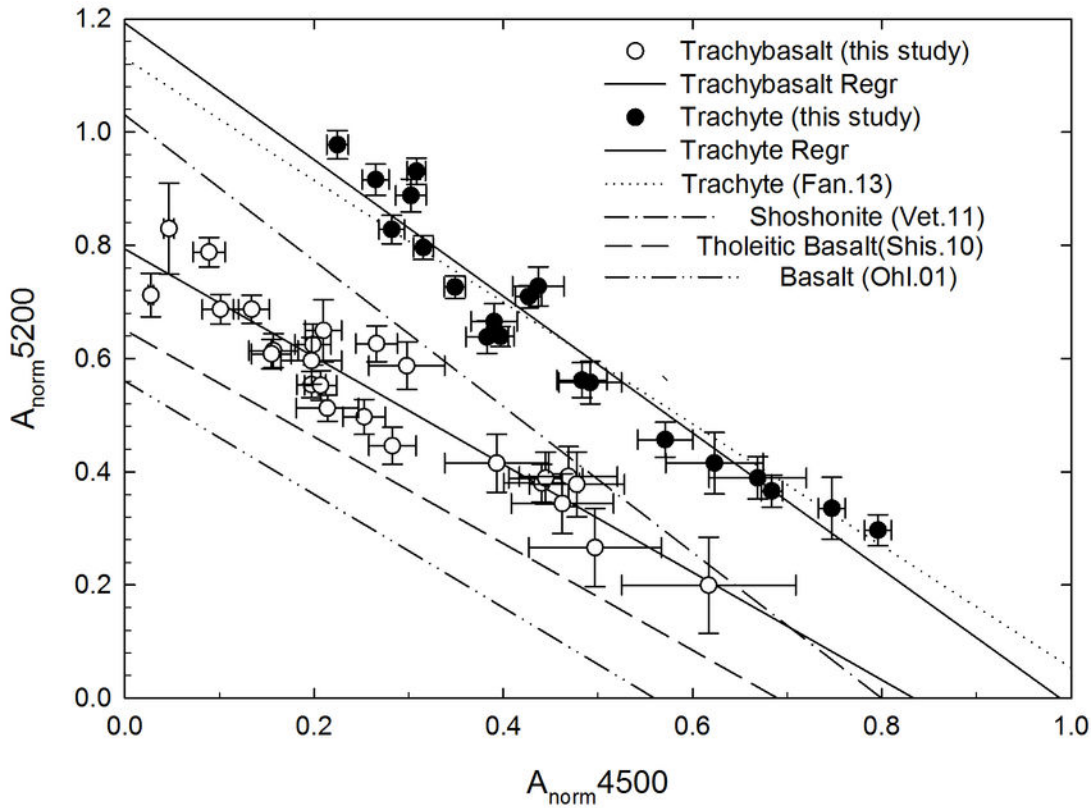


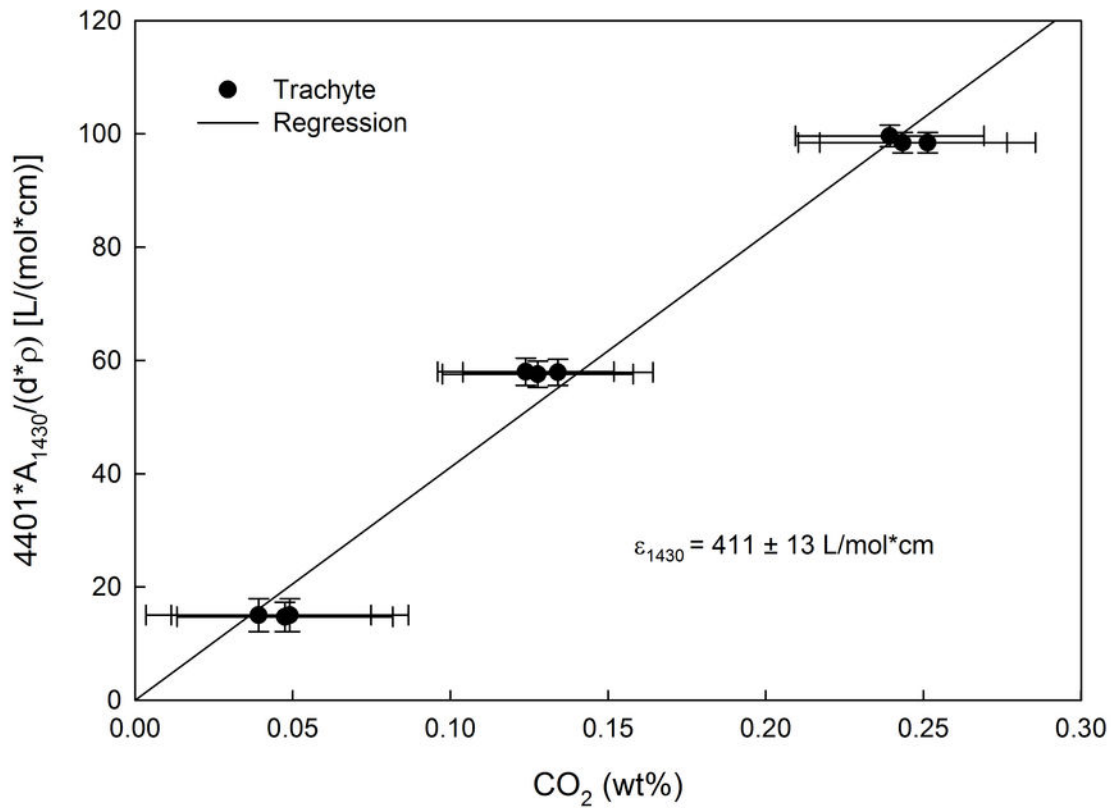
Stratigraphic type-section of the Campanian Ignimbrite around the city of Naples

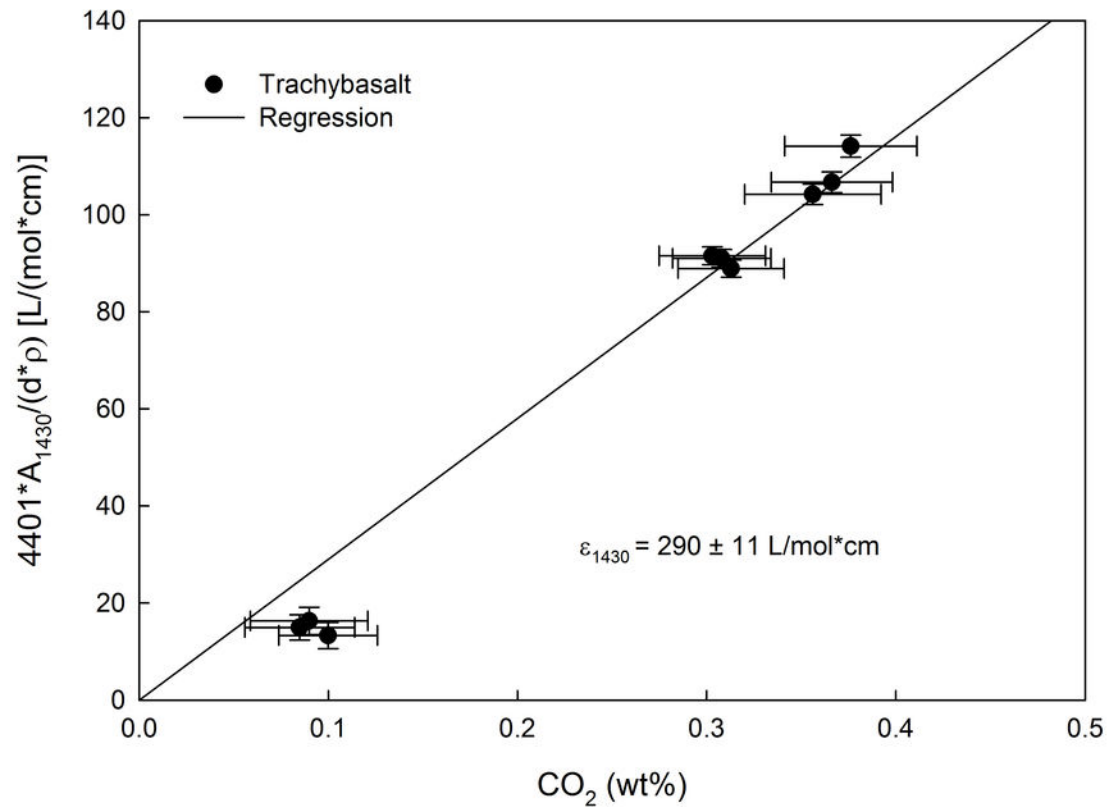
Campanian Ignimbrite Procida Island

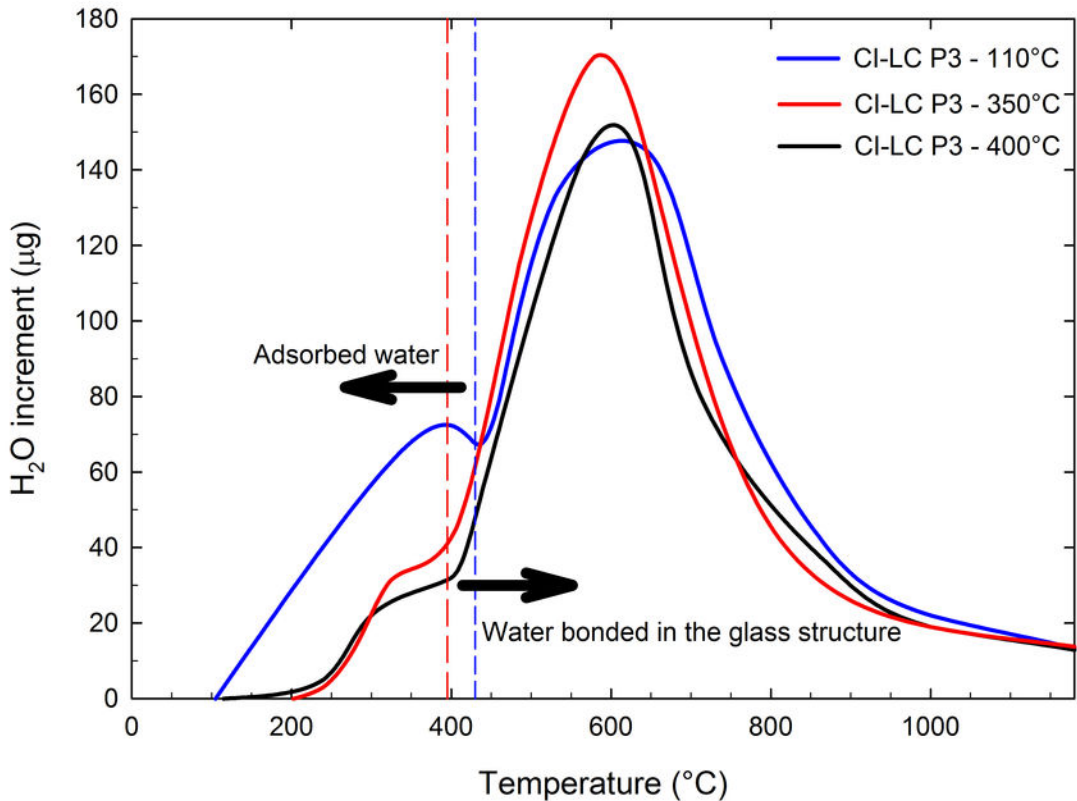
-  Ash
-  Pumice lapilli
-  Lithic clasts
-  Scoria spatter

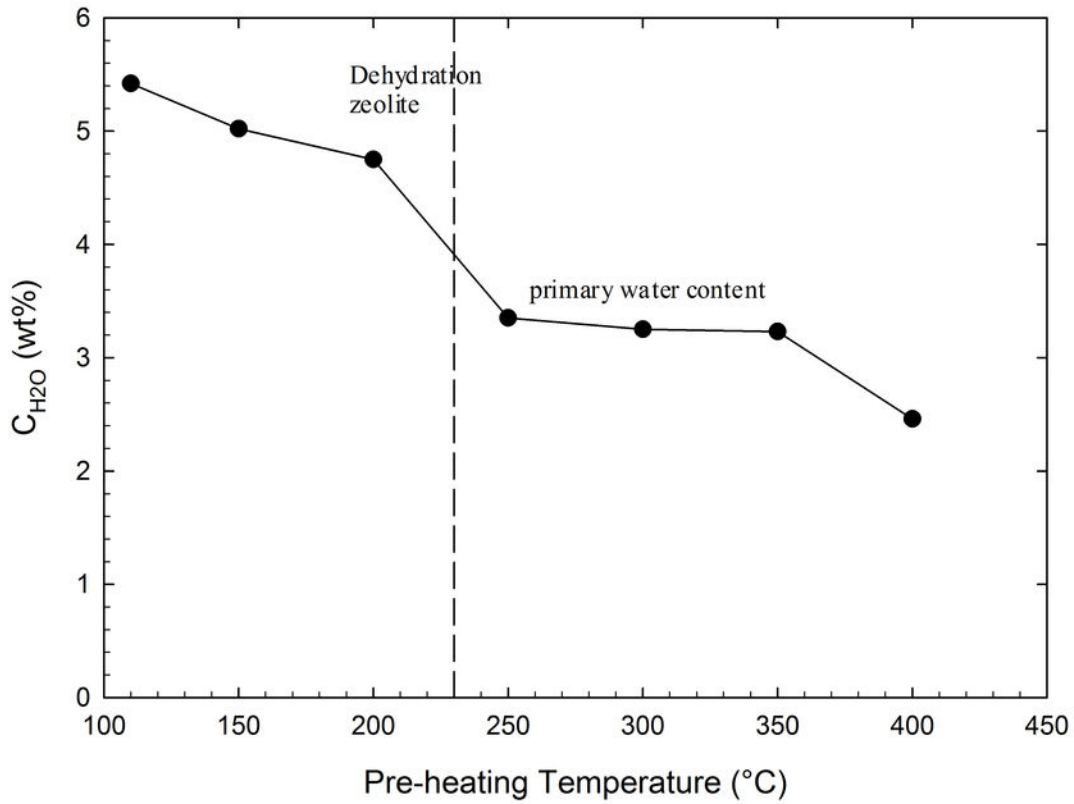


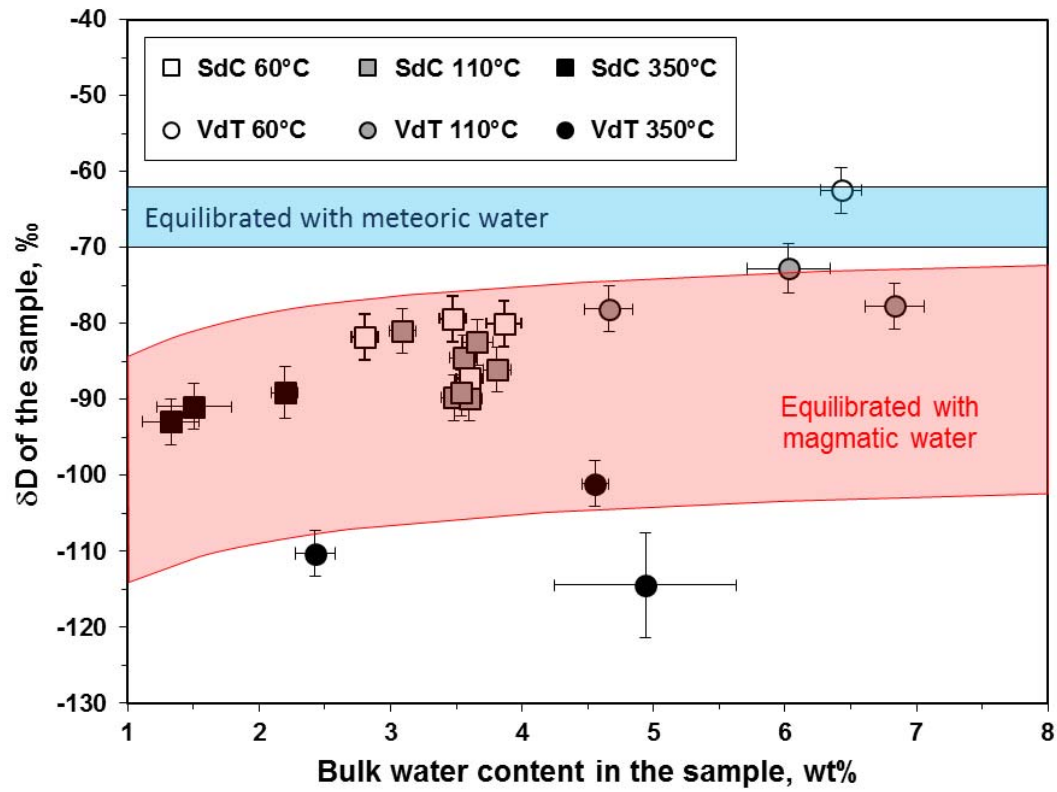


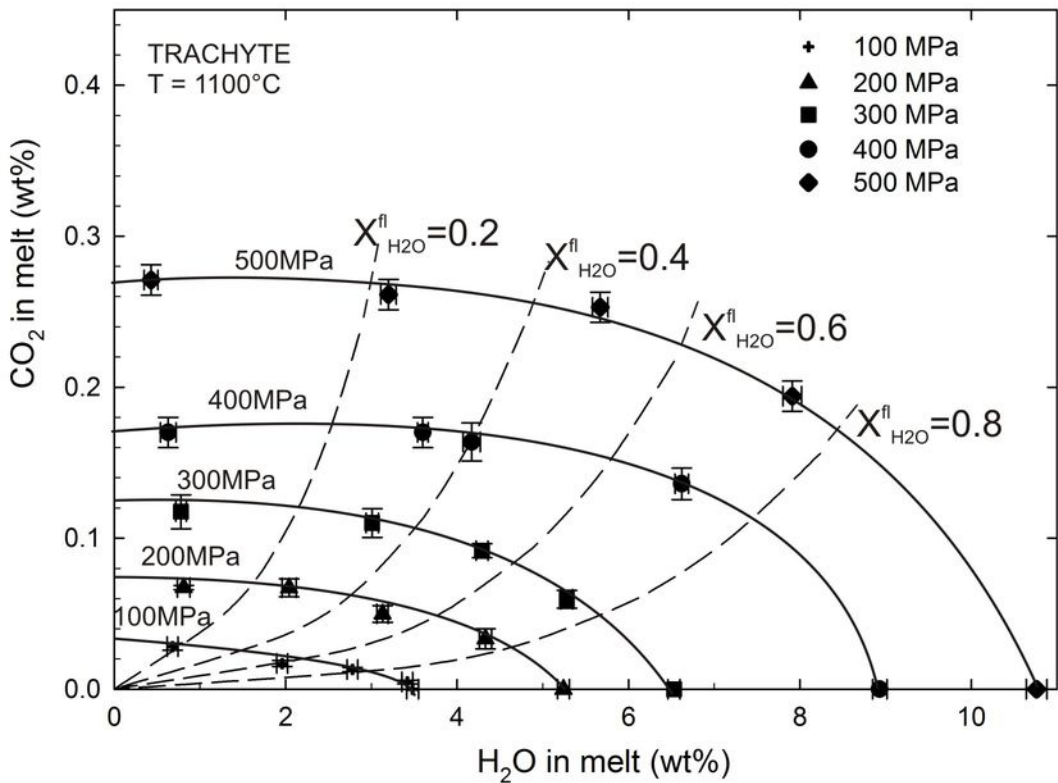


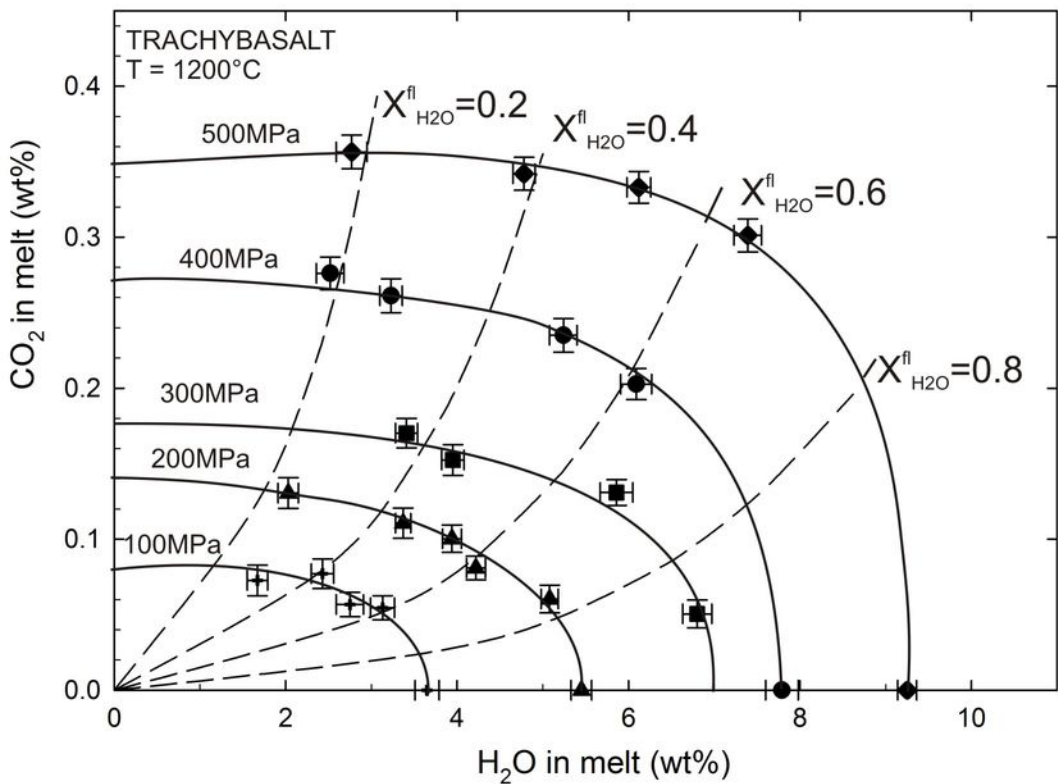


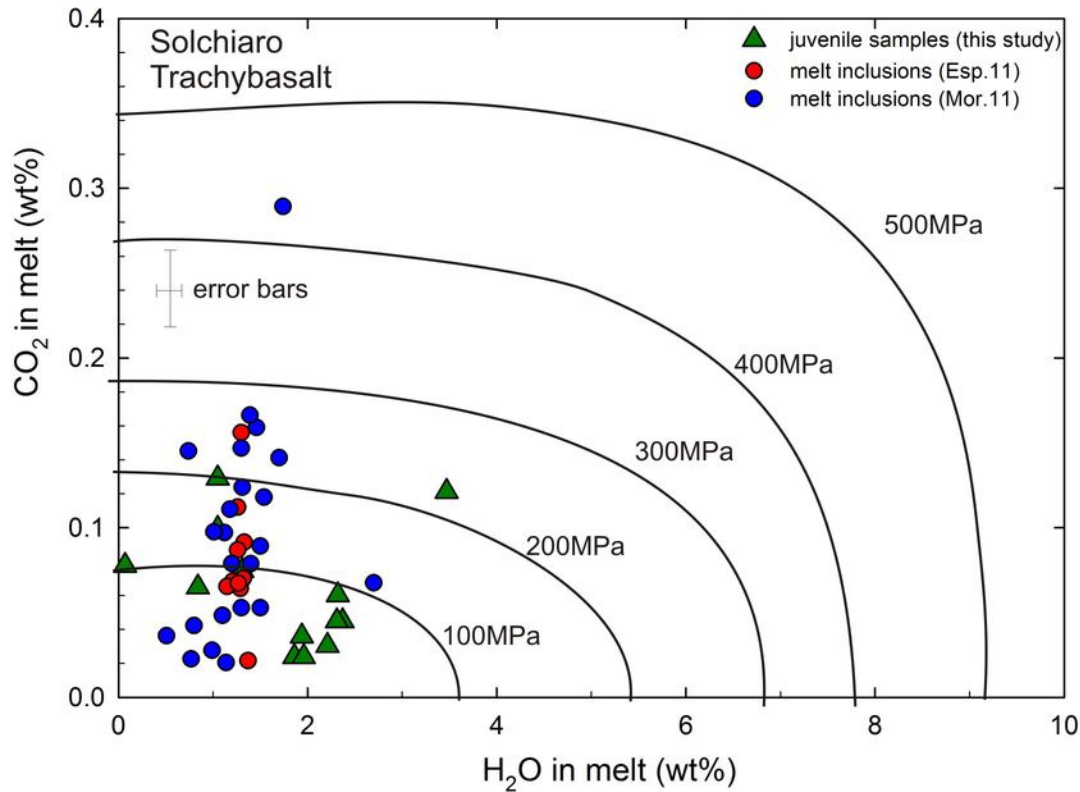












Revised Version

Table 1

Composition of trachytic and trachybasaltic melts measured by electron microprobe.

Sample	Trachyte	Trachybasalt
SiO ₂	60.31 (48)	49.03 (45)
TiO ₂	0.42 (1)	1.28 (12)
Al ₂ O ₃	18.32 (46)	16.10 (55)
FeO *	5.21 (16)	8.71 (61)
CaO	4.11 (10)	12.13 (48)
MgO	1.31 (13)	8.50 (34)
Na ₂ O	2.81 (16)	2.85 (19)
K ₂ O	7.47 (17)	1.56 (6)
Total	100.08	100.16
NBO/T	0.17	0.71

Notes. Microprobe analyses are based on 30 measurements on three fragments of each glass. One standard deviation is given in parentheses. * All iron is given as FeO.

Table 2 a Experimental conditions and results of H₂O and CO₂ solubility experiments for Trachyte

Sample	Pressure (MPa)	H ₂ O fluid (g)	CO ₂ fluid (g)	C _{H2O} KFT (wt%)	H ₂ O _m NIR (wt%)	OH NIR (wt%)	X _{H2O} ⁿ	CO ₂ MIR (ppm)	aH ₂ O Burn.04	aH ₂ O Aran.99
TA-1.1	100	0.00123	0.00003	3.48 (7)	1.27 (8)	2.31 (11)	1	0	0.88	1
TA-1.2	100	0.00164	0.00063	3.42 (6)	1.14 (10)	2.48 (7)	0.82	67 (12)	0.85	0.83
TA-1.3	100	0.00562	0.00510	2.78 (6)	0.97 (7)	1.73 (10)	0.71	130 (14)	0.64	0.73
TA-1.4	100	0.00226	0.00491	1.96 (6)	0.55 (7)	1.42 (10)	0.60	170 (20)	0.38	0.63
TA-1.5	100	0.00004	0.00599	0.68 (6)	0.35 (5)*	-	0.21	281 (24)	0.06	0.07
TA-2.1	200	0.00653	0.00006	5.24 (7)	3.17 (8)	1.87 (7)	1	0	0.97	1
TA-2.2	200	0.00345	0.00263	4.33 (7)	2.30 (4)	1.91 (4)	0.76	334 (67)	0.76	0.78
TA-2.3	200	0.00244	0.00379	3.13 (7)	1.46 (2)	1.57 (3)	0.59 ^s	498 (55)	0.50	0.63
TA-2.4	200	0.00108	0.00461	2.04 (8)	1.94 (1)	1.02 (10)	0.38	671 (60)	0.27	0.43
TA-2.5	200	0.00028	0.00303	0.81 (7)	0.45 (7)*	-	0.17	673 (14)	0.06	0.20
TA-3.1	300	0.00533	0.00009	6.53 (7)	4.44 (7)	2.55 (6)	1	0	0.99	1
TA-3.2	300	0.00301	0.00269	5.28 (7)	3.07 (5)	2.11 (6)	0.72	595 (59)	0.79	0.75
TA-3.3	300	0.00208	0.00351	4.06 (7)	2.10 (4)	2.19 (4)	0.58	917 (46)	0.62	0.63
TA-3.4	300	0.00115	0.00405	3.01 (7)	1.95 (4)	1.15 (5)	0.39 ^s	1100 (95)	0.39	0.45
TA-3.5	300	0.00031	0.00405	0.78 (6)	0.55 (6)*	-	0.12	1175 (112)	0.04	0.15
TA-4.1	400	0.00266	0.00005	8.93 (8)	6.27 (12)	2.54 (12)	1	0	1.16	1
TA-4.2	400	0.00235	0.00267	6.62 (8)	4.76 (10)	2.22 (11)	0.66	1360 (104)	0.83	0.70
TA-4.3	400	0.00131	0.00404	3.60 (10)	2.17 (8)	1.99 (10)	0.42	1637 (126)	0.49	0.49
TA-4.4	400	0.00094	0.00354	3.68 (6)	1.79 (8)	1.82 (10)	0.38 ^s	1685 (128)	0.42	0.45
TA-4.5	400	0.00009	0.00597	0.63 (9)	0.49 (7)*	-	0.06	1683 (128)	0.02	0.08
TA-5.1	500	0.00543	0.00003	10.76 (12)	7.97 (14)	2.69 (17)	1	0	1.29	1
TA-5.2	500	0.00324	0.00369	7.91 (11)	5.26 (12)	2.65 (16)	0.67 ^s	1940 (102)	0.91	0.72
TA-5.3	500	0.00119	0.00298	5.67 (9)	2.95 (18)	2.66 (15)	0.48 ^s	2530 (111)	0.63	0.54
TA-5.4	500	0.00050	0.00285	3.20 (9)	1.02 (9)	2.08 (13)	0.27	2613 (103)	0.31	0.34
TA-5.5	500	0.00005	0.00372	0.43 (8)	0.40 (7)*	-	0.06	2710 (99)	0.01	0.08

Table 2 b Experimental conditions and results of H₂O and CO₂ solubility experiments for Trachybasalt

Sample	Pressure (MPa)	H ₂ O fluid (g)	CO ₂ fluid (g)	C _{H2O} KFT (wt%)	H ₂ O _m NIR (wt%)	OH NIR (wt%)	XH ₂ O ⁿ	CO ₂ MIR (ppm)	aH ₂ O Burn.04	aH ₂ O Aran.99
TB-1.1	100	0.00069	0.00004	3.49 (7)	2.12 (17)	1.53 (12)	1	0	1.06	1
TB-1.2	100	0.00138	0.00163	2.93 (6)	1.59 (16)	1.54 (12)	0.66	545 (80)	0.84	0.68
TB-1.3	100	0.00103	0.00169	2.62 (15)	1.49 (17)	1.26 (12)	0.62	567 (80)	0.72	0.64
TB-1.4	100	0.00191	0.00366	2.27 (6)	1.23 (17)	1.20 (12)	0.55	772 (98)	0.58	0.57
TB-1.5	100	0.00131	0.00981	1.46 (13)	0.76 (16)	0.91 (14)	0.28	727 (102)	0.29	0.31
TB-2.1	200	0.00121	0.00013	5.28 (6)	3.86 (16)	1.59 (9)	1	0	1.16	1
TB-2.2	200	0.00029	0.00024	4.91 (10)	3.58 (13)	1.50 (9)	0.78	604 (92)	1.07	0.79
TB-2.3	200	0.00101	0.00205	3.22 (8)	1.98 (12)	1.39 (8)	0.50	1106 (100)	0.63	0.54
TB-2.4	200	0.00092	0.00210	3.78 (9)	2.46 (12)	1.48 (9)	0.60	1003 (90)	0.78	0.63
TB-2.5	200	0.00106	0.00855	1.87 (7)	1.08 (9)	0.95 (13)	0.20	1305 (102)	0.29	0.23
TB-2.6	200	0.00096	0.00099	4.08 (5)	2.94 (14)	1.28 (10)	0.66	809 (78)	0.86	0.69
TB-3.1	300	0.00049	0	6.63 (17)	5.35 (19)	1.45 (13)	0.93	505 (92)	1.19	0.93
TB-3.2	300	0.00088	0.00076	5.69 (19)	4.34 (18)	1.72 (13)	0.71	1309 (85)	1.00	0.74
TB-3.4	300	0.00109	0.00307	3.24 (13)	2.16 (17)	1.25 (12)	0.40	1703 (98)	0.51	0.45
TB-3.5	300	0.00102	0.00296	3.77 (13)	2.63 (17)	1.32 (13)	0.51	1525 (102)	0.62	0.56
TB-4.1	400	0.00104	0.00012	7.64 (19)	6.26 (22)	1.53 (17)	1	0	1.19	1
TB-4.2	400	0.00114	0.00168	5.91 (18)	4.60 (21)	1.49 (18)	0.64	2027 (102)	0.89	0.68
TB-4.3	400	0.00084	0.00158	5.07 (6)	3.89 (15)	1.35 (13)	0.53	2350 (111)	0.75	0.59
TB-4.4	400	0.00078	0.00368	3.08 (13)	1.94 (20)	1.29 (18)	0.29 ^s	2612 (111)	0.40	0.35
TB-4.5	400	0.00118	0.00991	2.35 (16)	1.45 (19)	1.07 (17)	0.19 ^s	2760 (109)	0.28	0.24
TB-5.1	500	0.00033	0.00003	9.10 (11)	7.40 (14)	1.85 (12)	1	0	1.28	1
TB-5.2	500	0.00074	0.00099	7.27 (16)	5.80 (12)	1.59 (16)	0.67	3012 (103)	0.99	0.71
TB-5.3	500	0.00109	0.00198	5.91 (14)	4.59 (18)	1.53 (15)	0.54	3330 (105)	0.79	0.60
TB-5.4	500	0.00122	0.00385	4.58 (13)	3.23 (9)	1.55 (11)	0.44	3420 (109)	0.59	0.51
TB-5.5	500	0.00105	0.00972	2.66 (18)	1.55 (17)	1.22 (15)	0.20	3565 (111)	0.29	0.26

Notes:

Calculated errors are shown in brackets near values.

Uncertainty in the weight of the content of H₂O and CO₂ in the fluid phase can reach 0.00010 g.

KFT value represents a single measurement with error calculated by error propagation considering error in titration rate of 0.02 mg/s, error in sample weight of 0.1 mg and uncertainty of unextracted water of 0.10 wt%.

Errors of the calculated contents of H₂O and CO₂, determined by IR, calculated by error propagation considering error of thickness (0.0002 cm), density (2% relative), reproducibility of absorbance (for each band respectively) and errors of the absorption coefficients. * H₂O contents determined by MIR.

X_{H₂O}^{fl} refers to the mole fractions of H₂O in fluid in the capsules after experiments.

Values were calculated by mass-balance when weight-loss procedure failed(§).

The water activity was calculated following the model of Burnham (1994) and the model of Aranovitch & Newton (1996).

Table 3

Deuterium content of selected pumices from CI eruption in comparison with their bulk water content.

Sample	H ₂ O - KFT (wt%) 25°C	H ₂ O - KFT (wt%) 110°C	H ₂ O - KFT (wt%) 50°C	H ₂ O – isot. (wt%) 60°C	H ₂ O – isot. (wt%) 110°C	H ₂ O – isot. (wt%) 350°C	δD (‰) 25°C	δD (‰) 110°C	δD (‰) 350°C
VdT-LB	8.82 (11)	5.49 (9)	3.77 (9)	6.50	5.9	4.5	-62 (0.1)	-73 (3.2)	-101 (1.7)
VdT-LD	-	6.73 (11)	3.86 (6)	-	7.0	4.5	-	-78 (0.5)	-114 (6.9)
VdT-LE2	-	4.28 (7)	2.49 (6)	-	4.8	2.5	-	-78 (0.9)	-109 (1.5)
SdC-A	3.50 (5)	3.39 (7)	1.26 (7)	3.50	3.4	1.7	-79 (0.1)	-90 (1.5)	-91 (2.4)
SdC-B	-	2.82 (6)	-	-	3.1	-	-82	-81 (0.6)	-
SdC-C	-	3.18 (8)	2.02 (6)	-	3.7	2.2	-87	-86 (0.7)	-89 (0.8)
SdC-D	3.29 (8)	3.64 (4)	1.40 (7)	3.80	3.7	1.5	-82 (1.9)	-82 (1.8)	-93 (3.4)

Notes.

Temperatures in the sample description refer to pre-heating.

- was not analyzed.

Calculated errors are shown in parentheses.

KFT value represents the average between at least two measurements. The error is calculated by error propagation considering error in titration rate of 0.02 mg/s, error in sample weight of 0.1 mg and uncertainty of unextracted water of 0.10 wt%. KFT measurements were performed on samples with grain size > 500 μm stored at room temperature (approx 25°C) and after a heating treatment at 110°C and 350°C for 4h.

Water contents from hydrogen isotopic analyses were evaluated based on signal intensity and are presented relative to NBS30 biotite.

The precision for δD is calculated ± 3%.